This document was prepared for the ETI by third parties under contract to the ETI. The ETI is making these documents and data available to the public to inform the debate on low carbon energy innovation and deployment.

Programme Area: Marine

Project: PerAWAT

Title: Tidal Coastal Basin Numerical Modelling: Large Scale Effects of Tidal Energy Extraction

Abstract:

This report is the fourth deliverable of Work Group 3 Work Package 3 from this project (WG3 WP3 D4). In this work package, EDF R&D adapted the numerical tools developed internally; Telemac-2D and Telemac-3D, in order to model the tidal farm performance and wake at large scales. This document presents the analysis of the results of tidal farm modelling on three sites modelled in WG3 WP3 D3: Paimpol-Bréhat, the Alderney Race, and the Pentland Firth. This analysis aims at characterising the hydrodynamic effects of tidal energy extraction at the basin scale, determining the tidal energy yield of each tidal farm layout. Tidal farm modelling is then discussed in order to identify the main limitations and the key sensitivities which may be further areas for development.

Context:

The Performance Assessment of Wave and Tidal Array Systems (PerAWaT) project, launched in October 2009 with £8m of ETI investment. The project delivered validated, commercial software tools capable of significantly reducing the levels of uncertainty associated with predicting the energy yield of major wave and tidal stream energy arrays. It also produced information that will help reduce commercial risk of future large scale wave and tidal array developments.

PerAWAT WG3 WP3 D4
Tidal coastal basin numerical modelling. Large scale effects of tidal energy extraction.

Project	PerAWAT
Work package	WG3
Deliverable	WG3 WP3 D4 - Tidal coastal basin numerical modelling. Large scale effects of tidal energy extraction.
Responsible author	Antoine Joly (EDF)
Other authors	Marc Andreewsky, Vanessa Martin, Sylvain Saviot, Chi-Tuân Pham (EDF)
Second reading	Charles Bodel, Marta Nogaj (EDF)
Circulation	Among all authors and readers
To be approved by	Robert Rawlinson-Smith (GH)
Date	21/11/2013
Issue	V1.0

Document revision history

Issue	Date	Summary
V0.1	05/11/2013	First draft
V0.2	21/11/2013	Comments from S. Parkinson taken into account
V1.0	21/11/2013	Final version

TABLE OF CONTENT

1 INTRODUCTION

1.1 Context of the report

The present report fits within the PerAWaT (**Per**formance **A**ssessment of **Wa**ve and **T**idal Array Systems) project which has been commissioned and funded by the **E**nergy **T**echnologies **I**nstitute (ETI). The aim of the project is to assess the large scale effects of tidal arrays (previously defined in WG3 WP3 D3) at basin scale. To do so, the outputs of the models developed in WG3 WP3 D3 are analysed. This report is the fourth deliverable of Work Group 3 Work Package 3 from this project (WG3 WP3 D4). In this work package, EDF R&D adapted the numerical tools developed internally; Telemac-2D and Telemac-3D, in order to model the tidal farm performance and wake at large scales.

1.2 Scope of this document

This document presents the analysis of the results of tidal farm modelling on three sites modelled in WG3 WP3 D3: Paimpol-Bréhat, the Alderney Race, and the Pentland Firth. This analysis aims at characterising the hydrodynamic effects of tidal energy extraction at the basin scale, determining the tidal energy yield of each tidal farm layout. Tidal farm modelling is then discussed in order to identify the main limitations and the key sensitivities which may be further areas for development.

Furthermore, the simulations for the three sites will be done for the same 16 days period, as this will provide consistency. Therefore all simulations will be performed from the 14th September 2001 to the 30th of September 2001. The first two days of the simulation are necessary to allow the flow to stabilise, and therefore one should really look at the results from the 16th of September 2001 onwards.

1.3 WG3 WP3 D4 Deliverables

a) Assessment Report: Large scale effects of tidal arrays at basin scale.

1.4 WG3 WP3 D4 Acceptance criteria

- Description and explanation of the numerical simulations for each UK site as defined in WG0 D2, and the hydrodynamic effects of tidal energy extraction at the basin scale.
- Quantitative assessment of the models abilities to accurately assess the tidal resource at each site.
- Discussion of the current valid applications and limitations of both models, and identifying key sensitivities which may be further areas for development.

2 THE ALDERNEY RACE

2.1 Introduction

Only available to PerAWaT participants.

3 THE PENTLAND FIRTH

3.1 Introduction

The aim of this study is to characterise the hydrodynamic effects of tidal energy extraction on the area of the Pentland Firth. The Pentland Firth separates the Orkney Islands from Caithness in the north of Scotland, see Figure 1. As illustrated by Figure 2, it is a region where strong tidal currents are experienced. The characterisation of the tidal conditions over this area is described in [A2]. The Pentland Firth has been acknowledged as being a site of particular interest for the possible deployment of industrial tidal turbine arrays.

Figure 1: The Pentland Firth location.

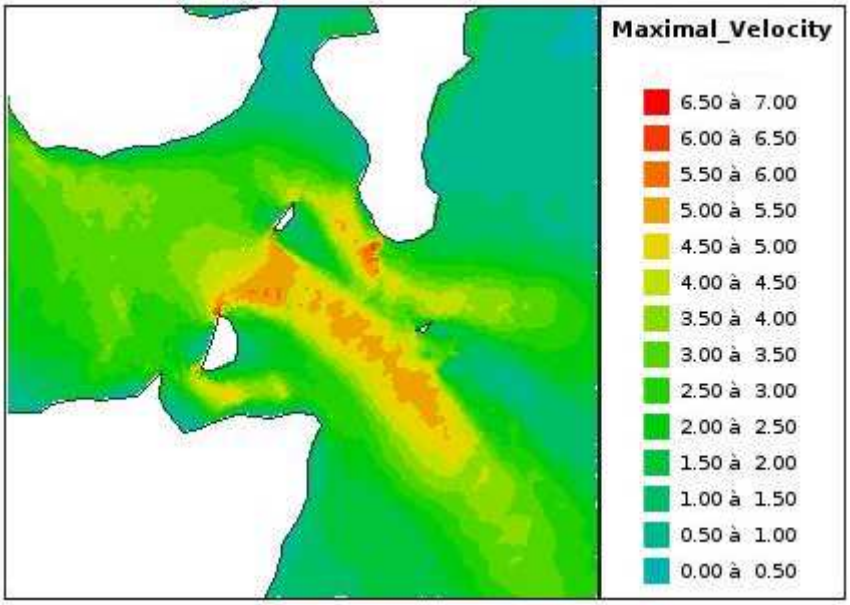

Figure 2: Maximal velocity in the Pentland Firth between the 14 of September and the 30 of September 2001. The data come from a Telemac-2D simulation with a validated model of the Pentland Firth.

3.2 Numerical modelling

3.2.1 Numerical models and tidal farm layouts

The numerical model of the Pentland Firth developed in WG3 WP3 D1 was used here for the simulation of the area including the tidal turbines.

The Telemac-2D version 6.2 software (available in open source since summer 2012) was used in [A3]. As described in [A2] § 4.2, the model is forced at its liquid boundaries by TPXO database.
The bathymetry coordinates follow a Mercator projection, with a centre of origin given by 0 degrees in longitude and 51.5 degrees in latitude (m).

The turbines were taken into account by adding a drag force in the momentum equation using the DRAGFO subroutine following the "global box" methodology [A3].

Three tidal farm layouts were defined (**Erreur ! Source du renvoi introuvable.**). The first farm (layout A) is composed of 73-turbine arrays (see Figure 3). The second farm (layout B) is composed of 2 rows of 14-turbine arrays (see Figure 4). The last configuration (layout C), consists in one significantly larger array of 250 turbines (see Figure 5). The location of the arrays of each layout is given in the following table:

Layout / configuration	Number of turbines	X begin (m)	X end (m)	Y begin (m)	Y end (m)
A : one row	73	-341979.9	-343232.6	1410993.4	1409506.8
B : first row	14	-343836.9	-344007.6	1409515.3	1409208.6
B : second row	14	-343681.3	-343843.0	1409429.7	1409118.1
C : one row	150	-341979.9	-346312.1	1410993.4	1405852.2

Table 1: Location of the tidal turbines arrays of each layout. The coordinates given here follow a Mercator projection, with a centre of origin given by 0 degrees in longitude and 51.5 degrees in latitude (m).

The following figures show the array locations for the 3 cases with the surrounding meshes used for the simulation:

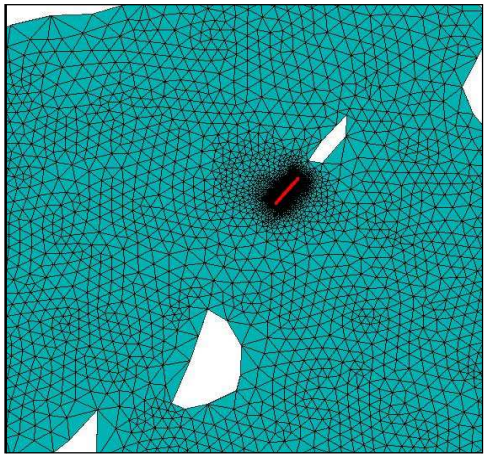

Figure 3: Location, in red, of the layout A in the Pentland Firth.

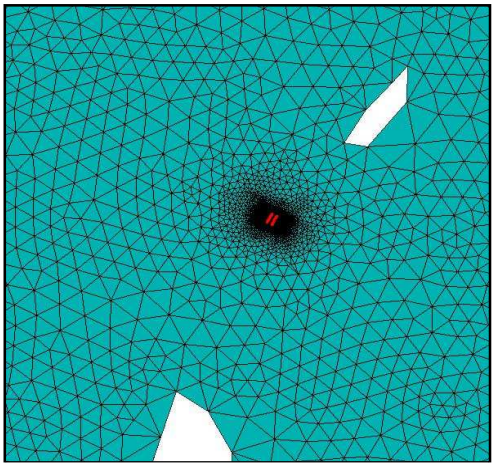

Figure 4: Location, in red, of the layout B in the Pentland Firth.

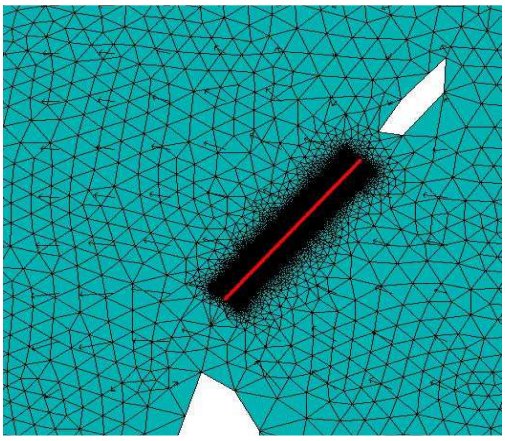

Figure 5: Location, in red, of the layout C in the Pentland Firth.

The transversal inter-device spacing (perpendicular to the main direction of the stream) is 27 m (1.5D) and the longitudinal inter-device spacing (stream wise), only for case B, is roughly equal to 180 m, (18D).

All turbines are assumed identical. Their diameter, D (m), their drag coefficient, C_d, and their power coefficient C_p, are supposed to be the same for each turbine and their values are D = 18 m, C_d = 0.86 and C_p = 0.53.

Three Pentland Firth models are built for each layout. Two "global boxes" are built to determine, for the layout A and C, the drag coefficient equivalent to each entire farm (see [A3]). For the layout B, since there are only 28 turbines each turbine is represented individually in the mesh. Nevertheless, in order to decrease the computation time, the time simulation is split in 7 parts.

3.2.2 Initial state

The initial state (without turbine) is the same for the three cases studied. Figure 7 shows the evolution of the depth-averaged tidal velocity and the free surface throughout the 14-day study period (starting from 16/09/2001 after a 2-days spin-up period, see [A3]) when no turbine is accounted for.

The following observations can be made:

- First slight increase of peak velocities from the 14th to the 18th Sept.
- Relatively stable period of maximal peak velocities from the 18th to 20th Sept.
- Clear decrease of peak velocities from the 20th to the 26th Sept.
- Relatively stable period of minimal peak velocities from the 26th to 28th Sept.
- Increase of peak velocities from the 28th Sept.
- Velocity during low tide (corresponding to each minimum of the free surface) is greater than the velocity during high tide.

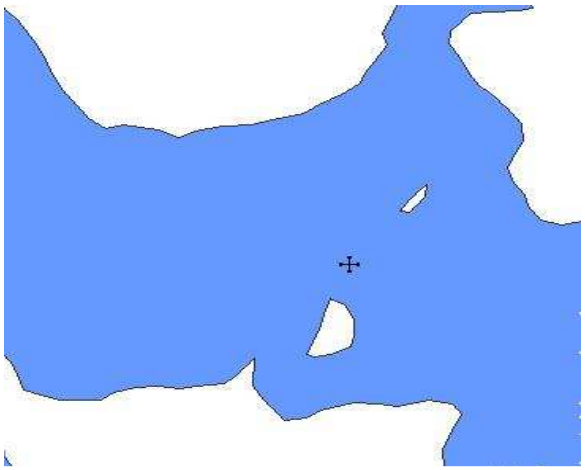

Figure 6: Selected point to observe the tidal evolution.

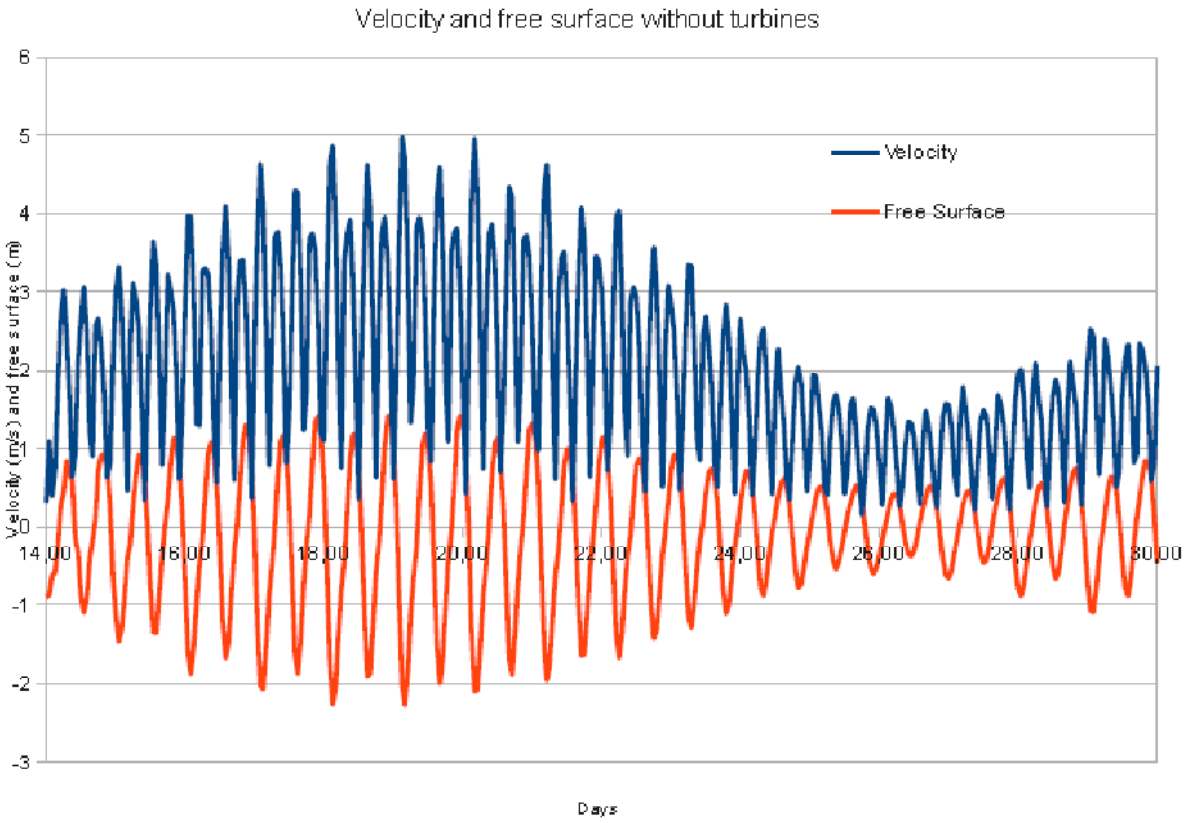

Figure 7: Velocity and free surface evolution observed at the selected point of Figure 6.

The most energetic tidal cycle, corresponding to a spring tide, runs the 19/09/2001 at about 3h00. The nearby islands constrain the orientation of the current and then, the ebb and flood current are systematically oriented towards South-East to North-West (or North-West to South-East), see Figure 8. The peak velocity reaches 4.97 m/s (at low tide). The second peak, about 25 hours later, is roughly equal to 4.95 m/s (at low tide also). The neap tide occurs the 26/09/2001 at about 10h00. In this case, peak velocities are much lower with top speeds simulated at 1.34 m/s (at low tide).

The undisturbed and disturbed (by tidal farms) flows will be compared on the identified spring tidal cycle. To complete the analysis, further comparisons between modelled flow with and without turbines will be carried out during the neap tide. The provided results during neap tide will only concern the main features.

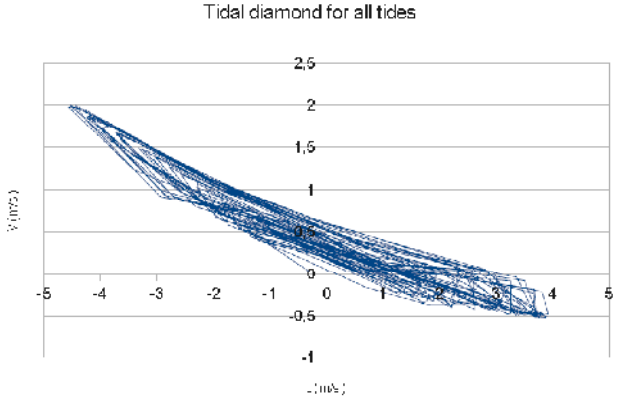

Figure 8: Tidal diamond for all tides.

3.3 Large scale effects of tidal arrays at basin scale

The hydrodynamic effects of tidal energy extraction are examined through a comparative study of tidal flow simulations with and without representation of tidal farm.

3.3.1 Tidal farm layout A

3.3.1.1 Global Box

The array of 73 turbines are modelled accordingly to the Global Box methodology as explained in WG3 WP3 D3 (cf. [A3] § 2.3). All turbines are individually modelled in a rectangular flume (whose dimensions are roughly about 1750 m x 2400 m), see Figure 9.

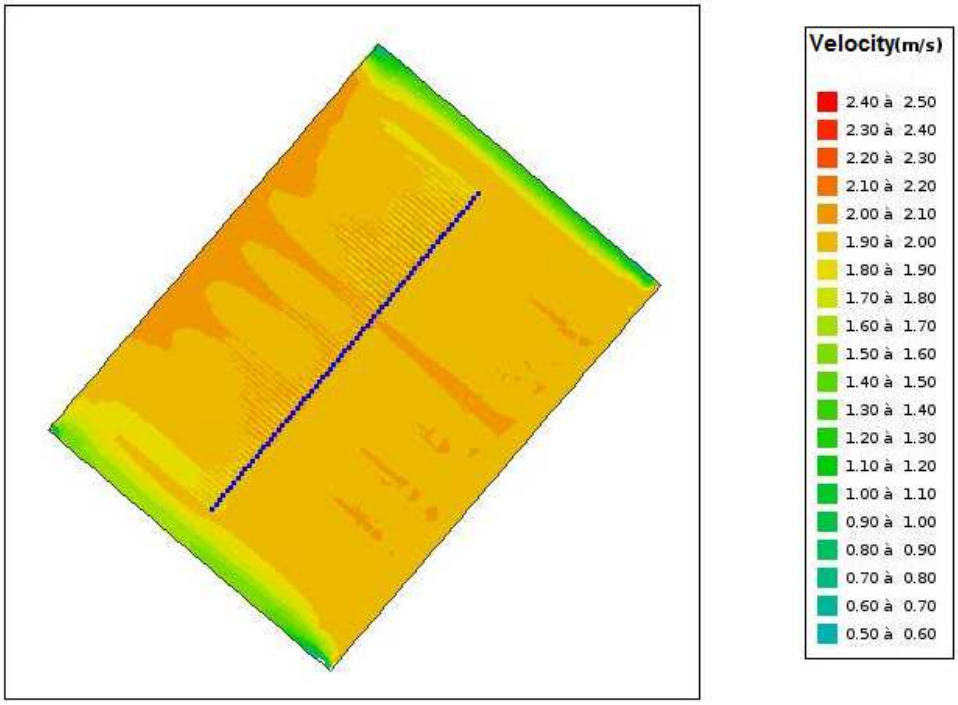

Figure 9: Velocity (m/s) observed with Layout A inside the global box.

Along the stream direction, the arrays are at least 800 m away from the boundary, corresponding to a distance of 45*D*, where *D* is the turbine diameter (here 18 m). Perpendicular to the stream direction, turbines are at a minimal distance of 220 m, i.e. 12*D* from the walls. The bathymetry of the canal is idealised. The bathymetry is homogeneously flat at a depth of 70 m. The inflow is imposed at a 2.0 m/s speed (a typical mean velocity near the Pentland Firth) and defines the upstream reference velocity.

The mechanical energy is then integrated throughout transversal sections of the canal. The obtained results are provided in Figure 10. The power variations (in MW) are indicated all along the longitudinal axis of the domain (blue curve). The energy loss solely due to the turbine action is derived from this curve by identifying the deficit of energy near the turbines location: Just upstream and downstream the gap, we localize points representing the middle of the oscillations of the power. Then, dE/dt is the difference between the values of those two points.

The resulting energy loss is estimated at 18.5 MW resulting in an equivalent drag coefficient Cd of 1.01 for the 73-turbine tidal farm by applying equation (8) of WG3WP3 D3 (cf. [A3] § 2.3).

The tidal farm is then modelled in Telemac-2D by applying the equivalent drag force in the area of a global box using the routine DRAGFO (see [A3] for more details).

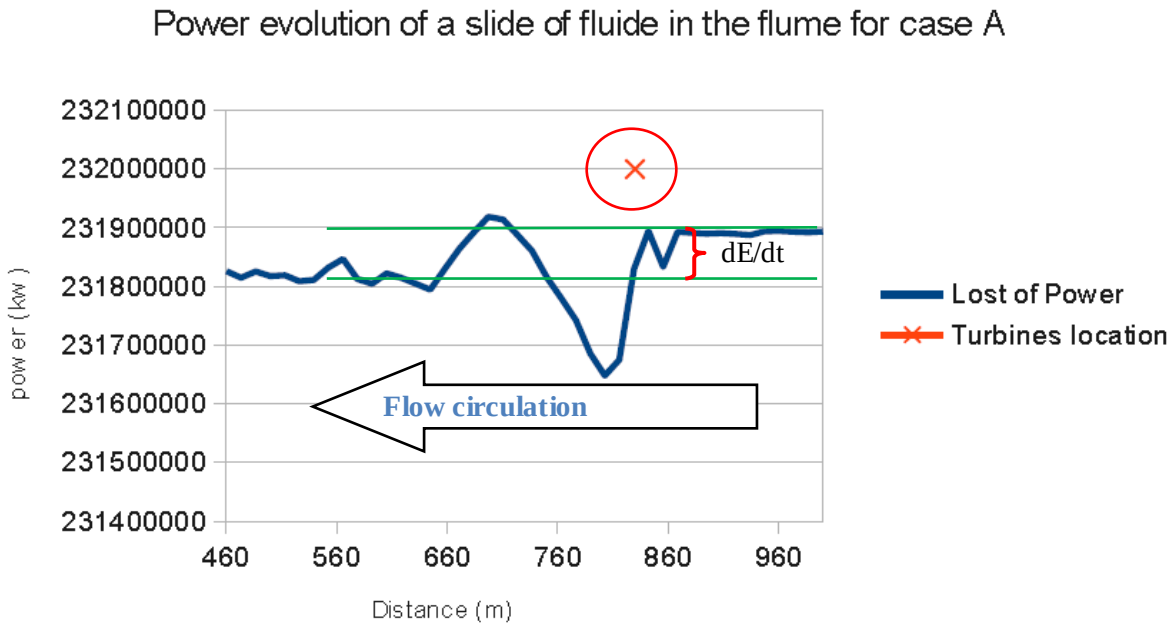

Figure 10: Variation of power[1] (MW) near the turbines location throughout the longitudinal axis of the global box domain (Blue curve). The circle surrounds the area where the turbines are located.

Note that, the flume has to be big enough to have enough space before and after the turbines in order to have a stable power curve just before and after the row of turbines.

3.3.1.2 Impact of tidal farm A

The turbines are represented by a single global box using the DRAGFO routine of Telemac-2D following the global box method (see [A3]). The flow is examined in details during the spring tide identified in the previous section and the main features are analysed during the neap tide.

3.3.1.2.1 Spring tide

The evolution of the perturbations induced by the tidal farm during the spring tide is illustrated by a series of hourly maps of the velocity difference, dV (m/s), between simulations with and without turbines ($dV = V_{\text{with TEC}} - V_{\text{without TEC}}$), displayed with the velocity vectors of the flow simulation accounting for turbines, see Figure 11.

The hydrodynamics effects of the tidal energy extraction results in the development of a wake downstream the farm which interacts with the surrounding islands and the coast and for which the shape and size of the wake can be sometimes not clearly identified. Especially, when the flow goes

[1] The power P(x) of a quantity of fluid passing through a section of a canal in one second has the following expression within the Saint-Venant equation:

$P(x) = \sum_{n=1}^{N} \left(\frac{V(x,y)^2}{2} + g.h(x,y) \right).V(x,y).h(x,y).\rho.ds$, where V is the absolute value of the velocity, h is the water depth, ds = dy.h(x,y), and ρ the water density. The sum is done over all discrete points along the transverse axis.

from the West to the East, the impact of the island and the surrounding coast is visible, but there is too much interaction with the islands and the coast for a clear wake structure to develop. Moreover, Figure 11 shows that tidal velocities are reduced near the turbine location with roughly a 15% reduction. When expressed in %, dV is calculated as follows: $dV = (V_{\text{with TEC}} - V_{\text{without TEC}}) / V_{\text{without TEC}}$. Significant velocity reductions (dV > 5 %) are experienced downstream of the farm until a distance roughly between 11 km and 13 km during the peak of ebb of the spring tide.

The impact is also characterised by some disturbance of flow in the surroundings, see Figure 12.
Moreover, the free surface (FS) is also impacted but the effects of the farm remain relatively low. The surface decreases downstream the farm and increases upstream (see Figure 16 and Figure 17). The maximal variations of free surface elevation are localised close to the farm and their amplitude are of the order of +/- 5-10 cm compared to the initial state. Nevertheless, it can be observed that during the flood and nearby the turbines, there is a place where the surface increases significantly (near 30 cm), see Figure 16.

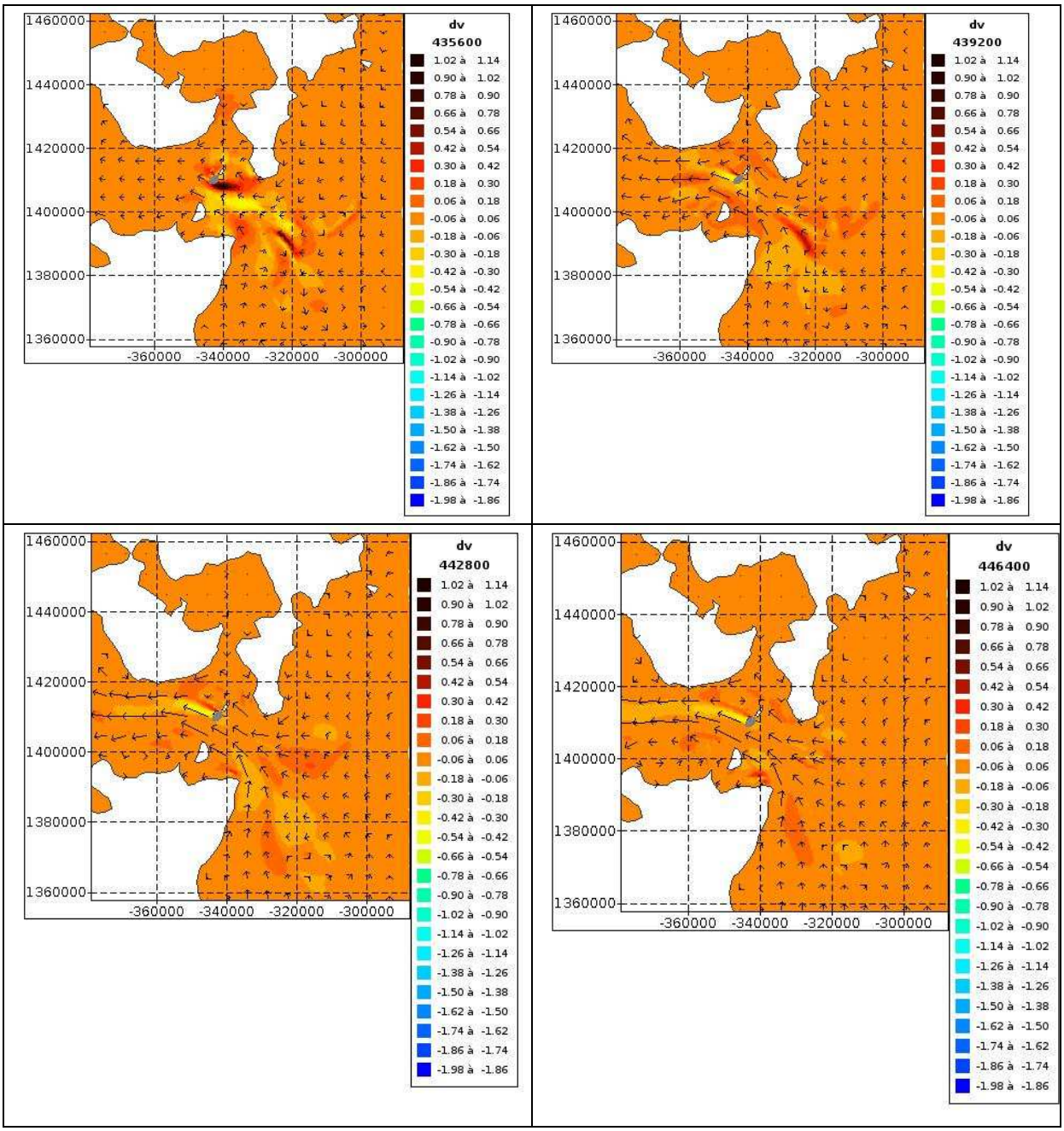

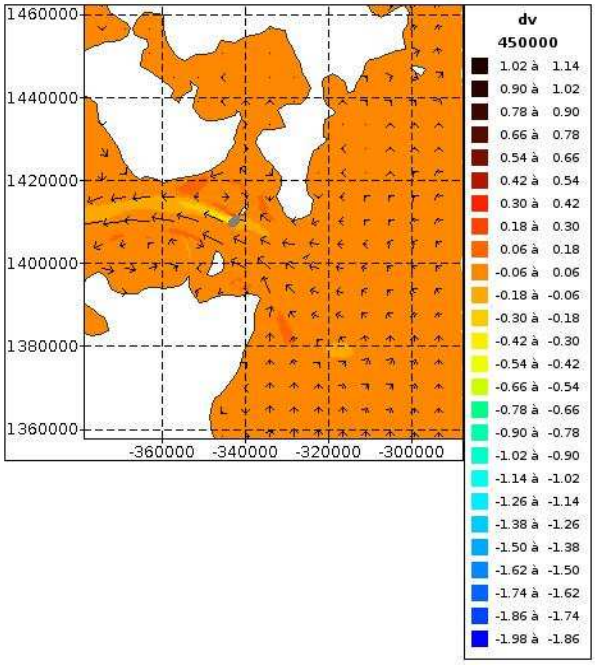
dv
450000
1.02 à 1.14
0.90 à 1.02
0.78 à 0.90
0.66 à 0.78
0.54 à 0.66
0.42 à 0.54
0.30 à 0.42
0.18 à 0.30
0.06 à 0.18
-0.06 à 0.06
-0.18 à -0.06
-0.30 à -0.18
-0.42 à -0.30
-0.54 à -0.42
-0.66 à -0.54
-0.78 à -0.66
-0.90 à -0.78
-1.02 à -0.90
-1.14 à -1.02
-1.26 à -1.14
-1.38 à -1.26
-1.50 à -1.38
-1.62 à -1.50
-1.74 à -1.62
-1.86 à -1.74
-1.98 à -1.86
1460000
1440000
1420000
1400000
1380000
1360000
-360000
-340000
-320000
-300000

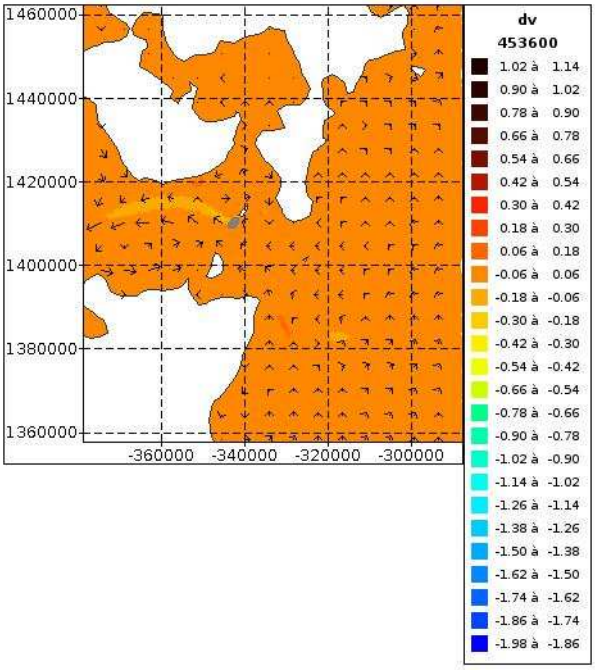
dv
453600
1.02 à 1.14
0.90 à 1.02
0.78 à 0.90
0.66 à 0.78
0.54 à 0.66
0.42 à 0.54
0.30 à 0.42
0.18 à 0.30
0.06 à 0.18
-0.06 à 0.06
-0.18 à -0.06
-0.30 à -0.18
-0.42 à -0.30
-0.54 à -0.42
-0.66 à -0.54
-0.78 à -0.66
-0.90 à -0.78
-1.02 à -0.90
-1.14 à -1.02
-1.26 à -1.14
-1.38 à -1.26
-1.50 à -1.38
-1.62 à -1.50
-1.74 à -1.62
-1.86 à -1.74
-1.98 à -1.86
1460000
1440000
1420000
1400000
1380000
1360000
-360000
-340000
-320000
-300000

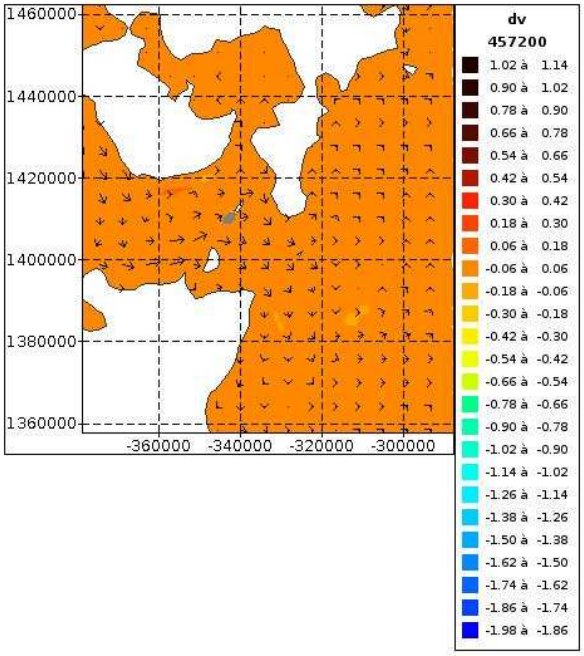
dv
457200
1.02 à 1.14
0.90 à 1.02
0.78 à 0.90
0.66 à 0.78
0.54 à 0.66
0.42 à 0.54
0.30 à 0.42
0.18 à 0.30
0.06 à 0.18
-0.06 à 0.06
-0.18 à -0.06
-0.30 à -0.18
-0.42 à -0.30
-0.54 à -0.42
-0.66 à -0.54
-0.78 à -0.66
-0.90 à -0.78
-1.02 à -0.90
-1.14 à -1.02
-1.26 à -1.14
-1.38 à -1.26
-1.50 à -1.38
-1.62 à -1.50
-1.74 à -1.62
-1.86 à -1.74
-1.98 à -1.86
1460000
1440000
1420000
1400000
1380000
1360000
-360000
-340000
-320000
-300000

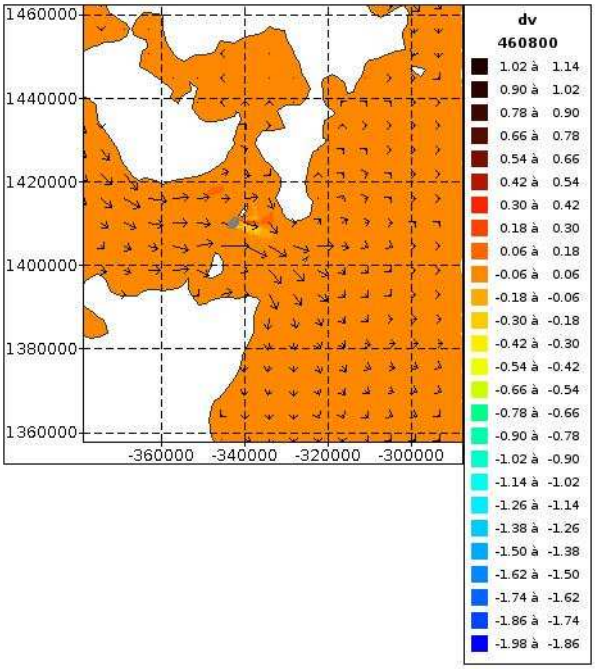
dv
460800
1.02 à 1.14
0.90 à 1.02
0.78 à 0.90
0.66 à 0.78
0.54 à 0.66
0.42 à 0.54
0.30 à 0.42
0.18 à 0.30
0.06 à 0.18
-0.06 à 0.06
-0.18 à -0.06
-0.30 à -0.18
-0.42 à -0.30
-0.54 à -0.42
-0.66 à -0.54
-0.78 à -0.66
-0.90 à -0.78
-1.02 à -0.90
-1.14 à -1.02
-1.26 à -1.14
-1.38 à -1.26
-1.50 à -1.38
-1.62 à -1.50
-1.74 à -1.62
-1.86 à -1.74
-1.98 à -1.86
1460000
1440000
1420000
1400000
1380000
1360000
-360000
-340000
-320000
-300000

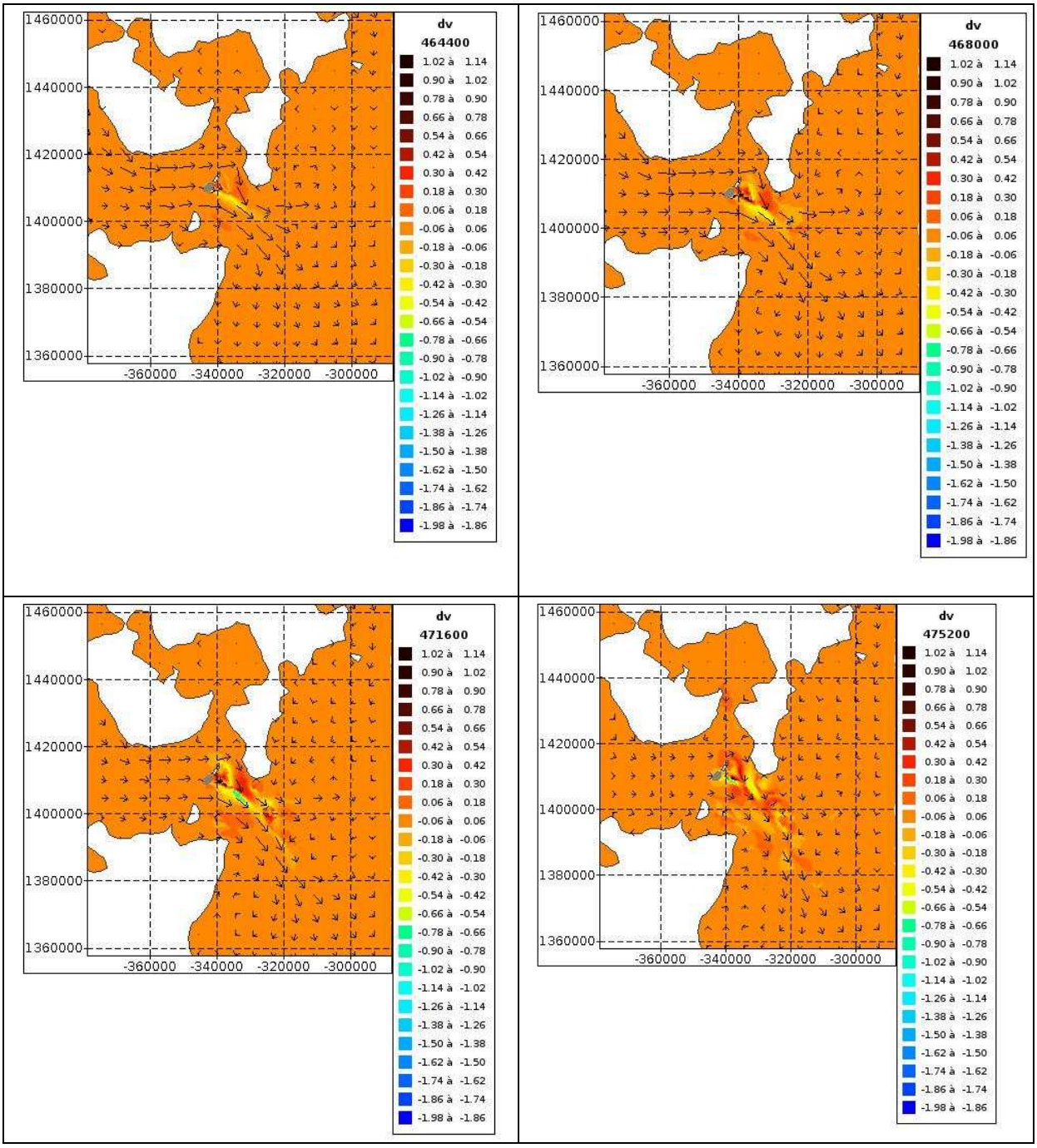
dv
464400
1.02 à 1.14
0.90 à 1.02
0.78 à 0.90
0.66 à 0.78
0.54 à 0.66
0.42 à 0.54
0.30 à 0.42
0.18 à 0.30
0.06 à 0.18
-0.06 à 0.06
-0.18 à -0.06
-0.30 à -0.18
-0.42 à -0.30
-0.54 à -0.42
-0.66 à -0.54
-0.78 à -0.66
-0.90 à -0.78
-1.02 à -0.90
-1.14 à -1.02
-1.26 à -1.14
-1.38 à -1.26
-1.50 à -1.38
-1.62 à -1.50
-1.74 à -1.62
-1.86 à -1.74
-1.98 à -1.86
1460000
1440000
1420000
1400000
1380000
1360000
-360000
-340000
-320000
-300000
dv
468000
1.02 à 1.14
0.90 à 1.02
0.78 à 0.90
0.66 à 0.78
0.54 à 0.66
0.42 à 0.54
0.30 à 0.42
0.18 à 0.30
0.06 à 0.18
-0.06 à 0.06
-0.18 à -0.06
-0.30 à -0.18
-0.42 à -0.30
-0.54 à -0.42
-0.66 à -0.54
-0.78 à -0.66
-0.90 à -0.78
-1.02 à -0.90
-1.14 à -1.02
-1.26 à -1.14
-1.38 à -1.26
-1.50 à -1.38
-1.62 à -1.50
-1.74 à -1.62
-1.86 à -1.74
-1.98 à -1.86
1460000
1440000
1420000
1400000
1380000
1360000
-360000
-340000
-320000
-300000
dv
471600
1.02 à 1.14
0.90 à 1.02
0.78 à 0.90
0.66 à 0.78
0.54 à 0.66
0.42 à 0.54
0.30 à 0.42
0.18 à 0.30
0.06 à 0.18
-0.06 à 0.06
-0.18 à -0.06
-0.30 à -0.18
-0.42 à -0.30
-0.54 à -0.42
-0.66 à -0.54
-0.78 à -0.66
-0.90 à -0.78
-1.02 à -0.90
-1.14 à -1.02
-1.26 à -1.14
-1.38 à -1.26
-1.50 à -1.38
-1.62 à -1.50
-1.74 à -1.62
-1.86 à -1.74
-1.98 à -1.86
1460000
1440000
1420000
1400000
1380000
1360000
-360000
-340000
-320000
-300000
dv
475200
1.02 à 1.14
0.90 à 1.02
0.78 à 0.90
0.66 à 0.78
0.54 à 0.66
0.42 à 0.54
0.30 à 0.42
0.18 à 0.30
0.06 à 0.18
-0.06 à 0.06
-0.18 à -0.06
-0.30 à -0.18
-0.42 à -0.30
-0.54 à -0.42
-0.66 à -0.54
-0.78 à -0.66
-0.90 à -0.78
-1.02 à -0.90
-1.14 à -1.02
-1.26 à -1.14
-1.38 à -1.26
-1.50 à -1.38
-1.62 à -1.50
-1.74 à -1.62
-1.86 à -1.74
-1.98 à -1.86
1460000
1440000
1420000
1400000
1380000
1360000
-360000
-340000
-320000
-300000

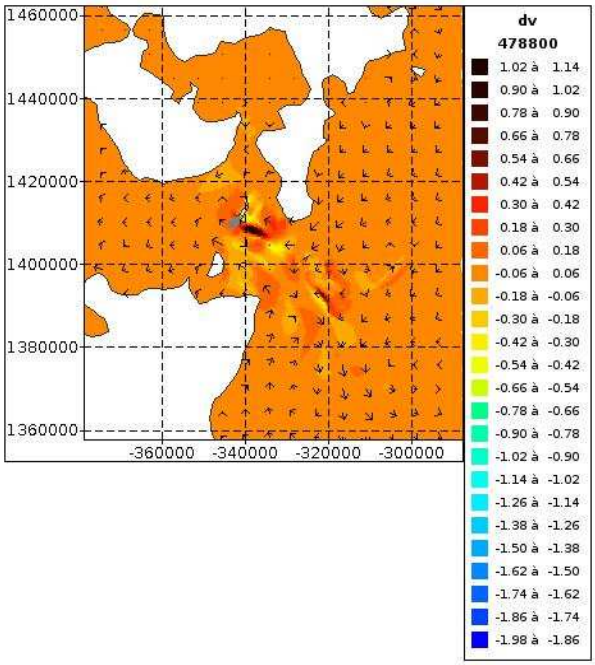

Figure 11: Hourly maps of the velocity difference dV (m/s) (dV = $V_{with\ TEC}$ - $V_{without\ TEC}$) and tidal velocity vectors of the flow simulated with turbines (black arrows). The gray shape is the tidal turbines.

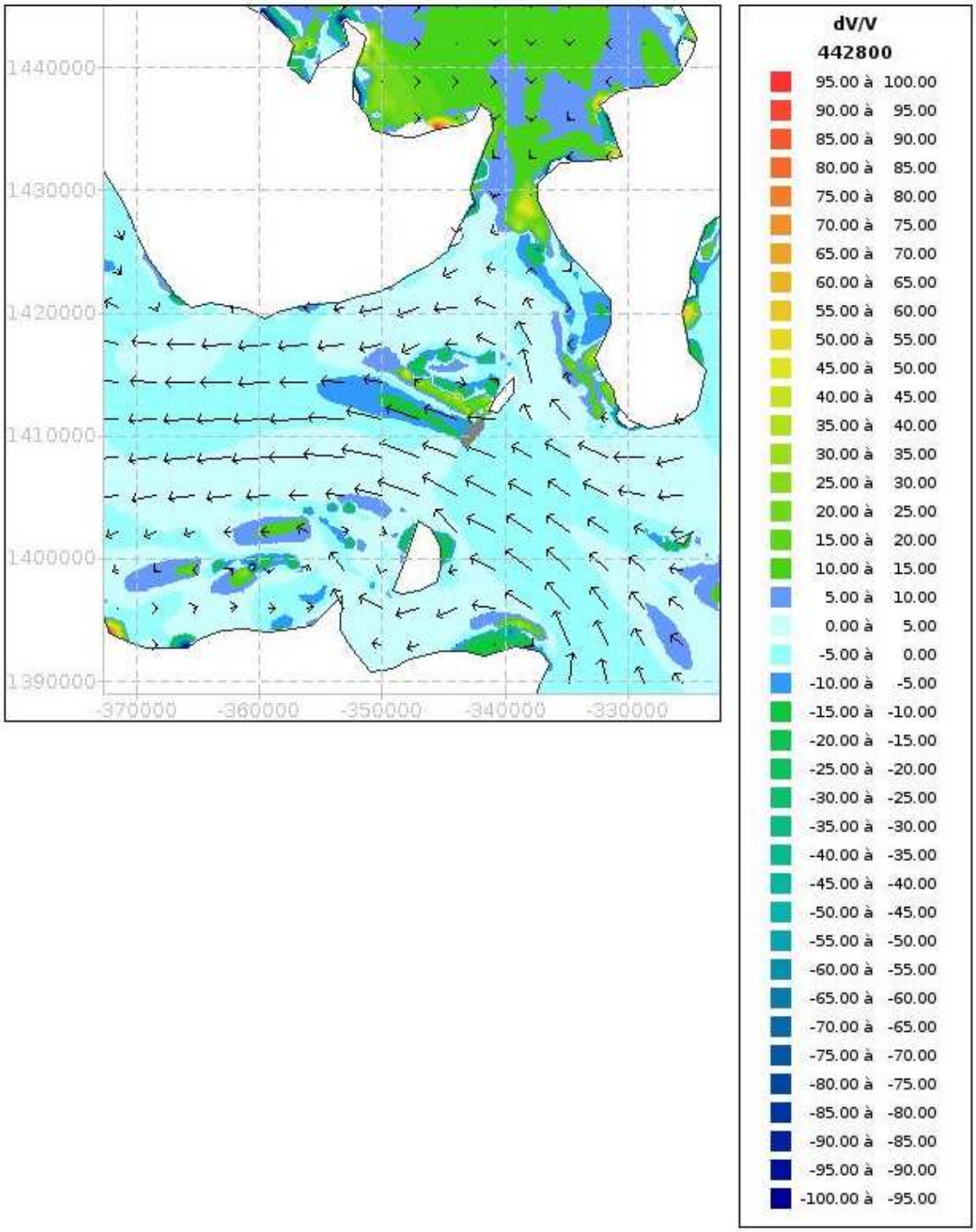

Figure 12: Relative variation of the velocity observed when the current velocity (at low tide) is maximal. The gray shape is the tidal turbines. The wake is roughly equal to 13 km.

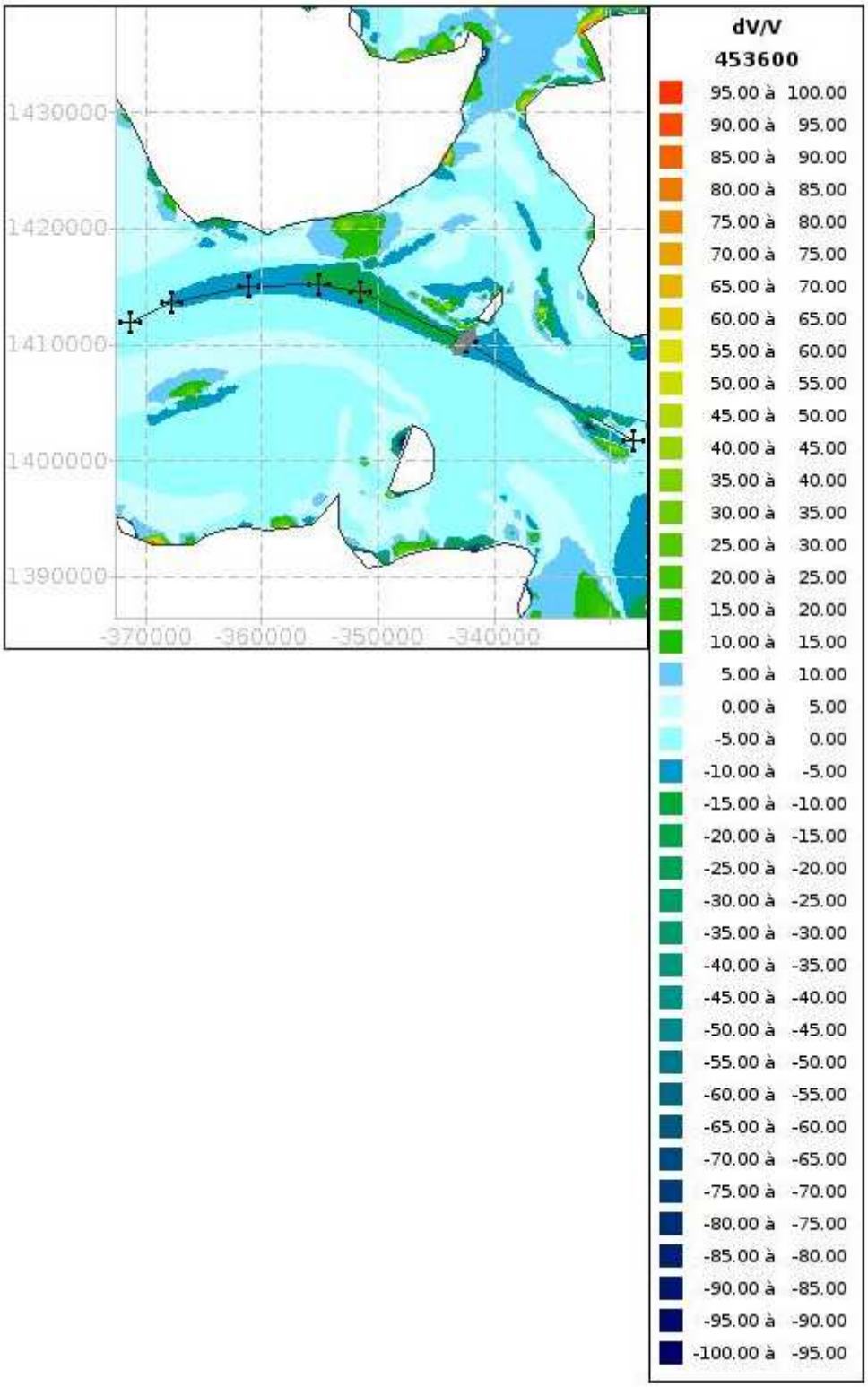

Figure 13: Relative variation of the velocity. Maximum wake length observed 3 hours after the maximal current velocity (at low tide). The gray shape is the tidal turbines.

In Figure 13 the wake is greater than in Figure 12 but it can be noted that, 3 hours after the maximal current velocity, the velocity has decreased a lot (which can create a bias in the relative velocity).

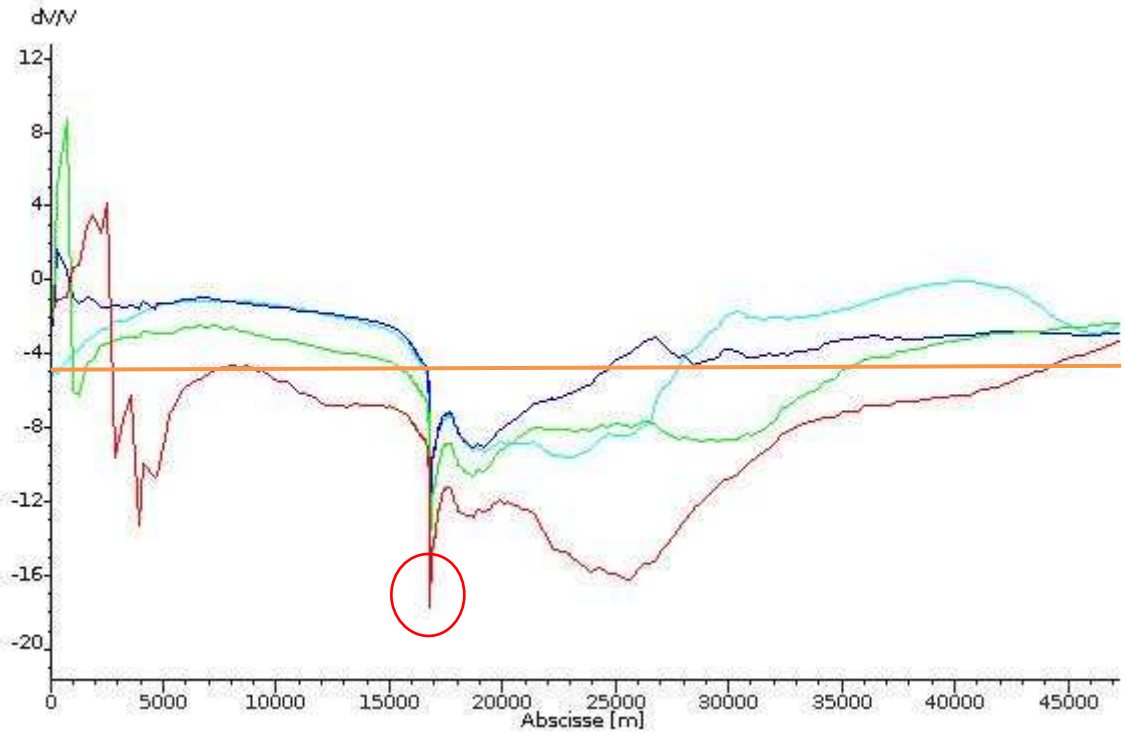

Figure 14: Reduction (in %) in tidal current velocity along the wake of layout A tidal farm at low tide. Line in light blue: maximum of tidal velocity (occurring at time h); blue line: tidal velocity at h+1 hour; green line: tidal velocity at h+2 hours; red line: tidal velocity at h+3 hours. The red circle shows the velocity deficit at the turbines location and the orange line shows a 5% deficit.

In Figure 13, the distance from the turbine where the velocity is equal to 95% of the initial velocity is about 27 km. The row of turbine is 2 km long, and then the wake is roughly equal to 13.5x(length of the row turbines). Nevertheless, it's perhaps more relevant to evaluate the wake when the tidal velocity is maximal. In this case (the light blue in Figure 14), the wake is between 11 km and 13 km.

As we can see Figure 14 and Figure 13, there is also an impact on the velocity deficit located upstream from the turbines.

Figure 13 shows the difficulties to evaluate the wake just after the high tide. The presence of the islands surrounding and the coast explains the observed perturbations. For example, the wake is drawn in Figure 15 one hour after the high tide:

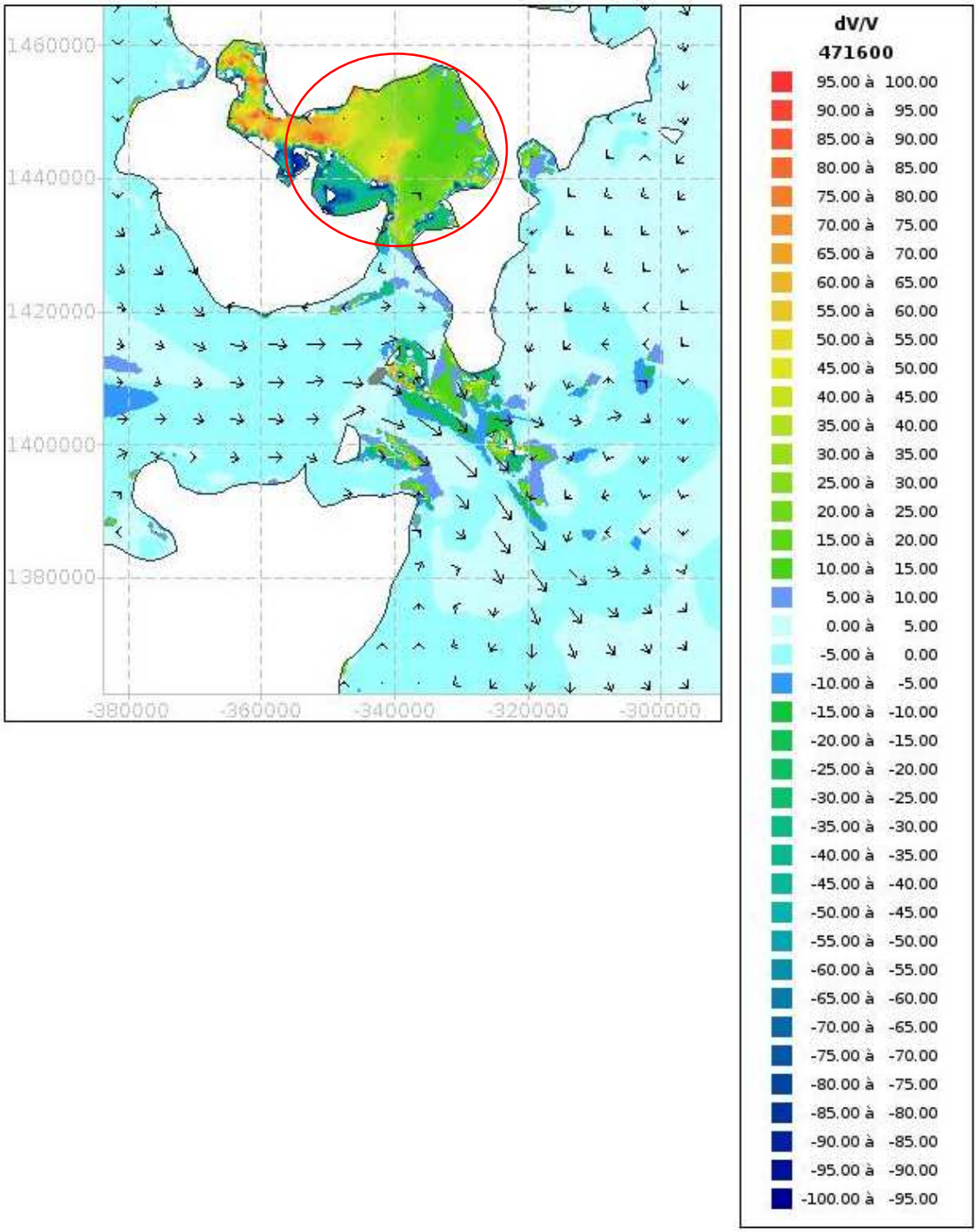

Figure 15: wake observed 1 hour after the high tide. The gray shape is the tidal turbines. The red circle is an example of an area where the velocity vectors have a small size.

Note that, to interpret the Figure 15, one has to pay attention to the length of the velocity vectors. If the vectors of the velocity are small, then the relative variations, even if it is high, do not have a relevant significance (see the area delimited by the red circle in Figure 15).

The wake is also very disturbed at each hour just after the high tide, and then the length of the wake can't really be estimate in these cases.

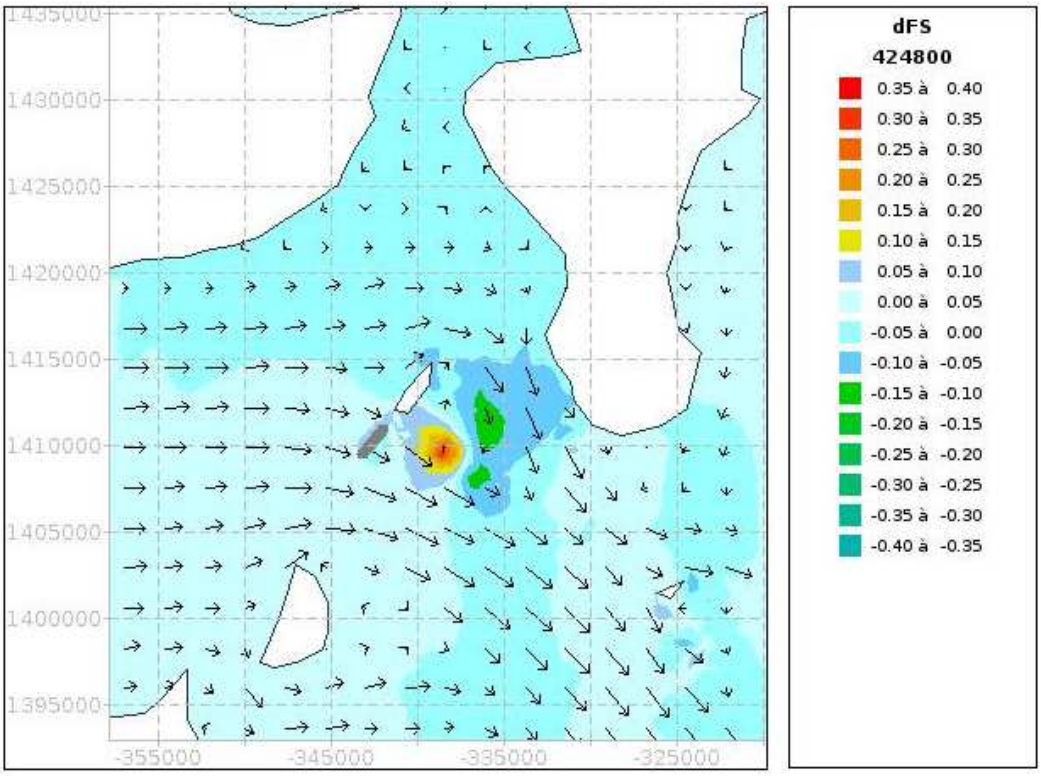

Figure 16: Difference in free surface, dFS (m), during flood (one hour after the maximal velocity) - location of tidal turbines (gray line).

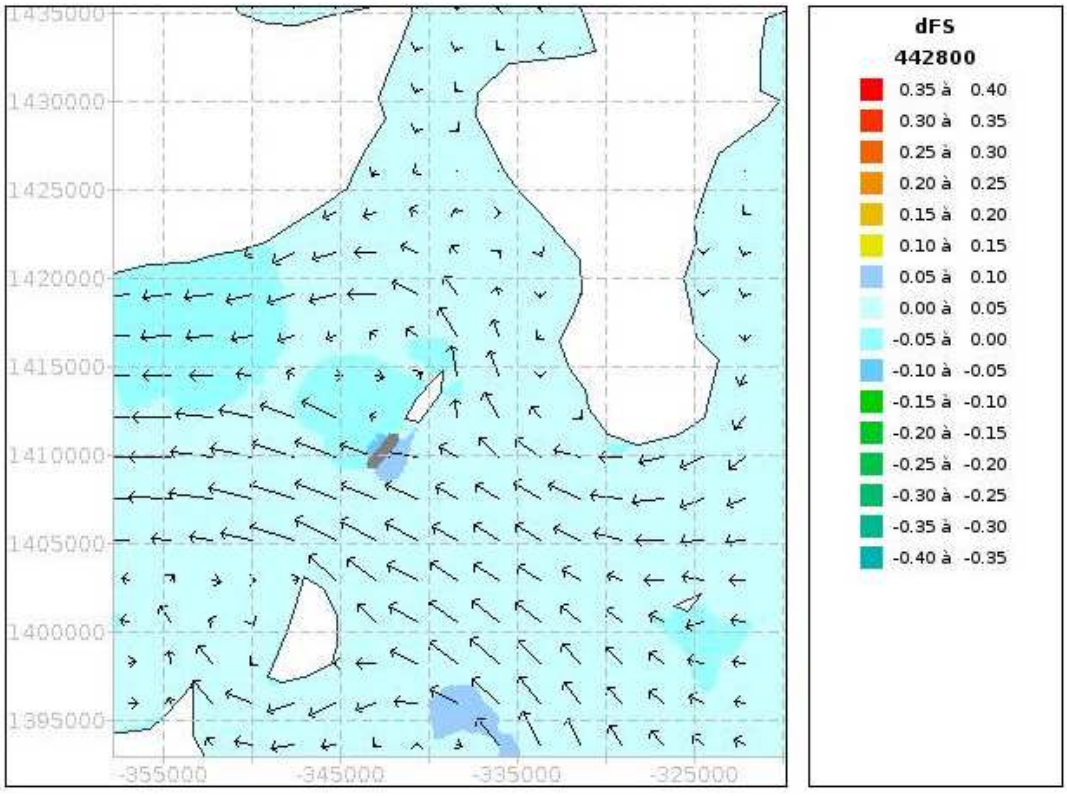

Figure 17: Difference in free surface, dFS (m), during ebb (at the maximal velocity) - location of tidal turbines (gray line).

3.3.1.2.2 Neap tide

The main characteristics of the disturbances of the flow induced by the farm are the same as the ones described in the previous sub-section. At ebb, wakes are around 11.5 km until the velocity deficit becomes lower than 5 % of the initial flow conditions. During the flood, the wake is much smaller and around 2km. Absolute velocity differences are much lower but the relative differences (expressed in %) along spatial profiles are similar.

Differences in free surface elevations are much smaller with variations of maximal amplitude of +/- 0.05 m.

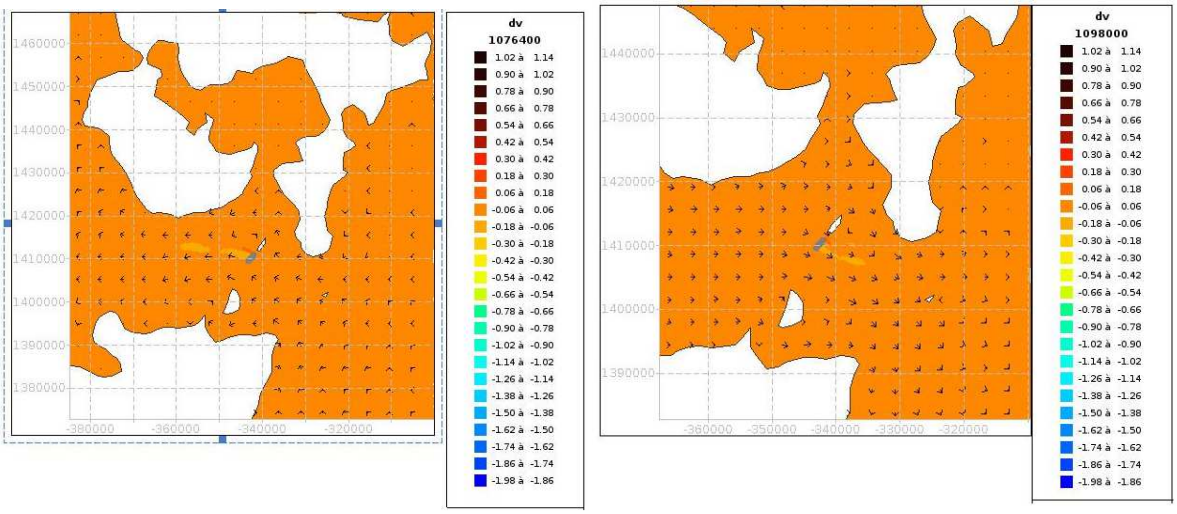

Figure 18: Wake downstream the tidal farm during the peak of ebb (left panel) and flood (right panel) of the neap tide.

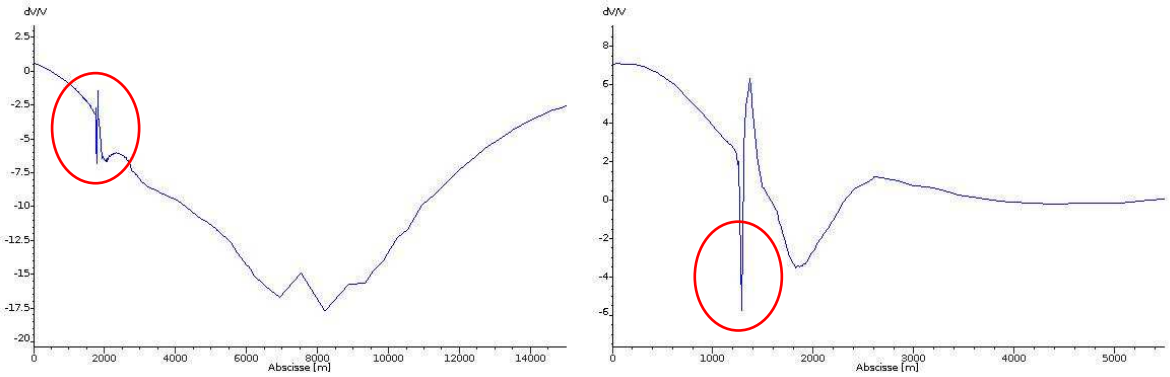

Figure 19: Evolution of tidal current velocity along the wake of layout A tidal farm during the ebb (left panel) and flood (right panel) tide. The red circle is located at the turbine location.

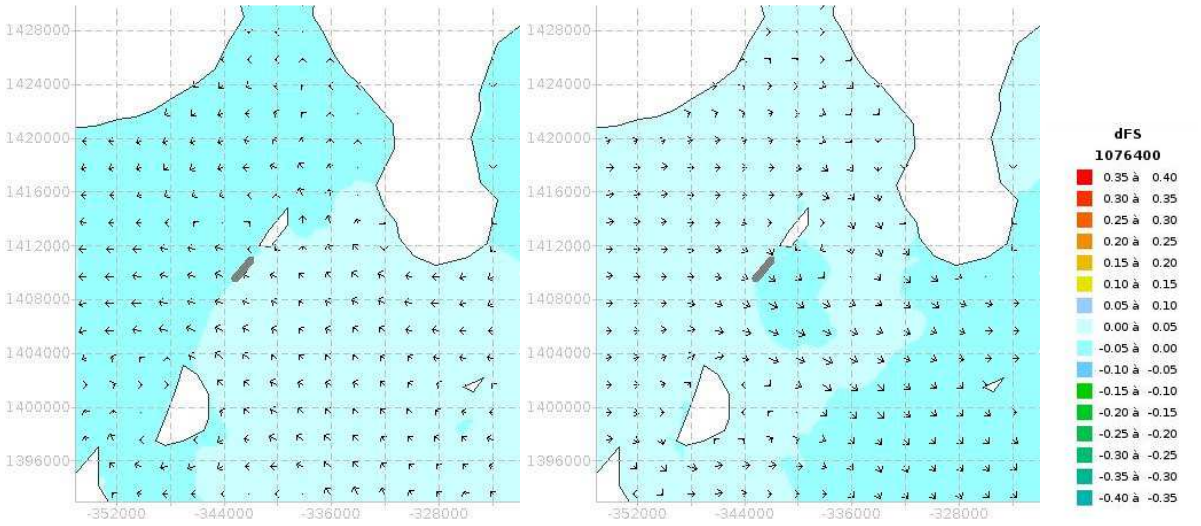

Figure 20: Difference in free surface, during ebb (left panel) and flood tide (right panel) - location of tidal turbines (gray line).

3.3.1.2.3 Power

This section describes the power evolution observed with the "Quasi-Bubble" option set in Telemac-2D. To illustrate the importance of using "Quasi-bubble" elements a comparison will be given for the power simulated with and without this option of Telemac-2D.

The evolution of the tidal farm power (in W) follows the variations of the current intensity (see Figure 21) with highest power outputs during the spring tide and lowest power during the neap tide. However, intensities fluctuations are dramatically amplified as power depends on the cube of the velocity.
The time-averaged power is roughly equal to 50 MW (equivalent to 0.68 MW/TEC). The power reaches a peak at 3.2 MW/TEC during spring tide, which should be compared to a "peak" power below 0.2 MW/TEC during the flood of the neap tide.

Finally, a ten percent difference in the mean power is observable with and without the "Quasi-Bubble" option.

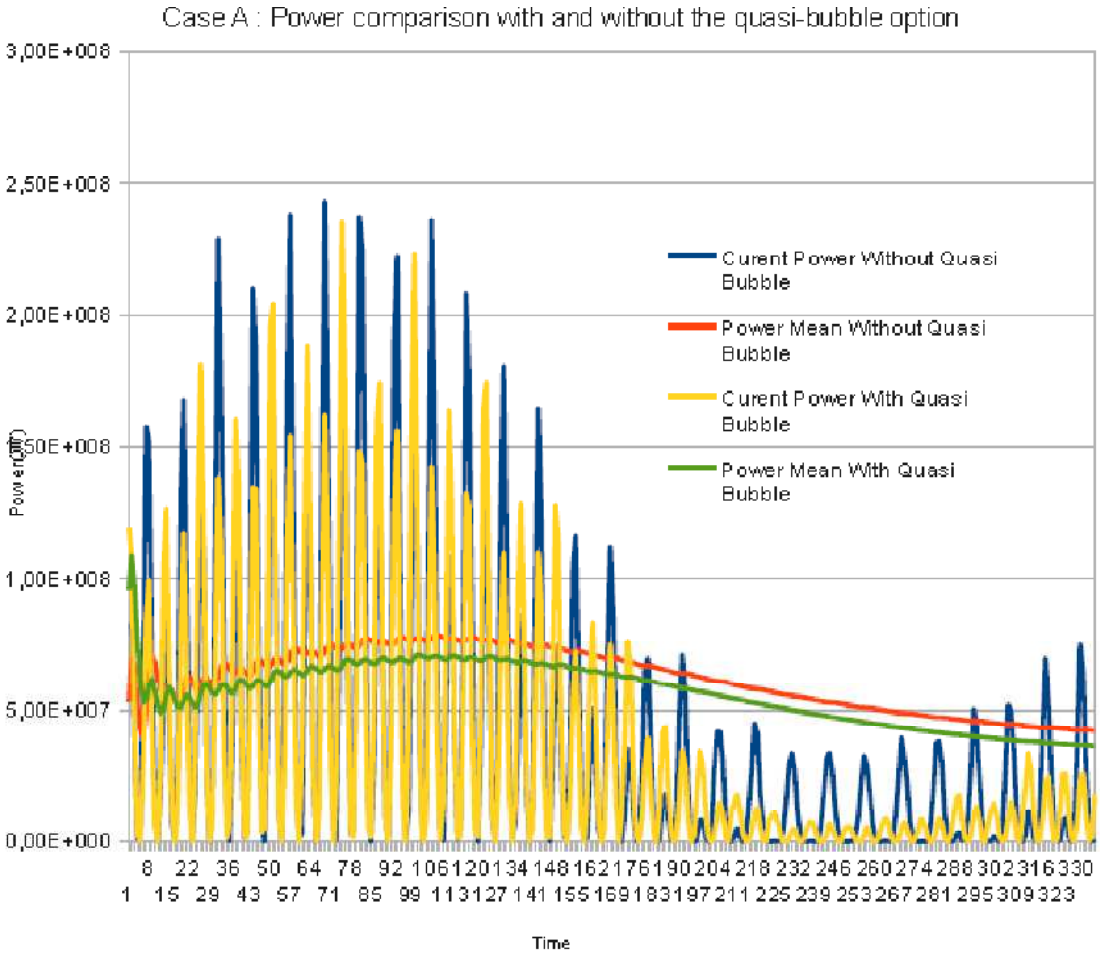

Figure 21: Comparison for case A between mean and current power for two kinds of simulations, the first one without the Telemac-2D quasi-bubble option, the second one with the Telemac-2D quasi-bubble option.

Note that, if the "Quasi-Bubble" option doesn't change so much the amount of the extracted energy, this option is clearly interesting to analyse the wake, as simulations solved without this option give very instable flow fields.

3.3.2 Tidal farm layout B

Here, each turbine is represented by a box (so 28 boxes are used) using the DRAGFO routine of Telemac-2D following the recommended method (see [A3]). The flow is examined in details during the spring tide identified in the previous chapter and the main features are analysed during the neap tide.

3.3.2.1 Individual representation of each turbine

Figure 22 shows the individual wake corresponding to each turbine:

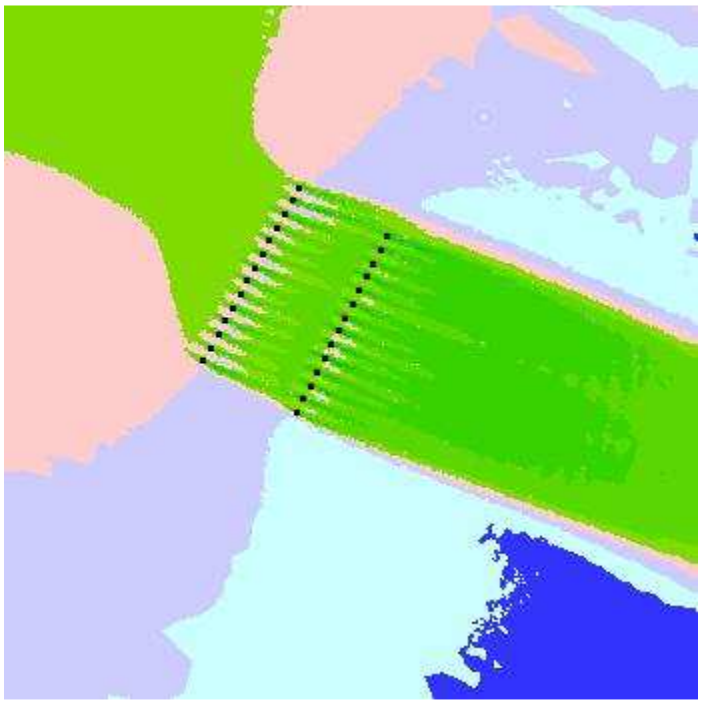

Figure 22: individual wake corresponding to each turbine.

Since the Big Box methodology has not been used the defined drag coefficient (Cd equal to 0.86) has been used directly.

3.3.2.2 Impact of tidal farm B

3.3.2.2.1 Spring tide

The evolution of the perturbations induced by the tidal farm during the spring tide is illustrated by a serie of hourly maps of the velocity difference, dV (m/s), between simulations with and without turbines ($dV = V_{with\ TEC} - V_{without\ TEC}$), displayed with the velocity vectors of the flow simulation accounting for turbines in Figure 23.

The hydrodynamic effects of the tidal energy extraction results in the development of a wake downstream the farm. Those effects are much smaller than the one seen in the previous case “farm A”. When the flow goes from the West to the East, the impact of the interaction of the island and the surrounded coast is not really visible (unlike case A). Moreover, Figure 25 shows that tidal velocities are reduced near the turbine location with roughly a 25% of reduction. This velocity reduction is higher than what was obtained for the case A. This can certainly be explained by the fact that in this case B we have two rows of turbines. When expressed in %, dV is calculated as follows: $dV = (V_{with\ TEC} - V_{without\ TEC}) / V_{without\ TEC}$. Significant velocity reductions (dV > 5 %) are experienced downstream of the farm for up to 10 km during the peak of ebb or the spring tide. The row length is about 380 m, and for this case there are 2 rows. So, the cumulative size of the rows is about 760 m. Then, the maximum wake length is roughly 13 times the dimension of the cumulative size. We get a similar result as the one obtained in case A.

The effects of the farm on the free surface (FS) remain relatively low (see Figure 26), less than 5 cm of differences. No other large scale effects were observed apart localised numerical noise perturbations (see section 3.3.2.2.3).

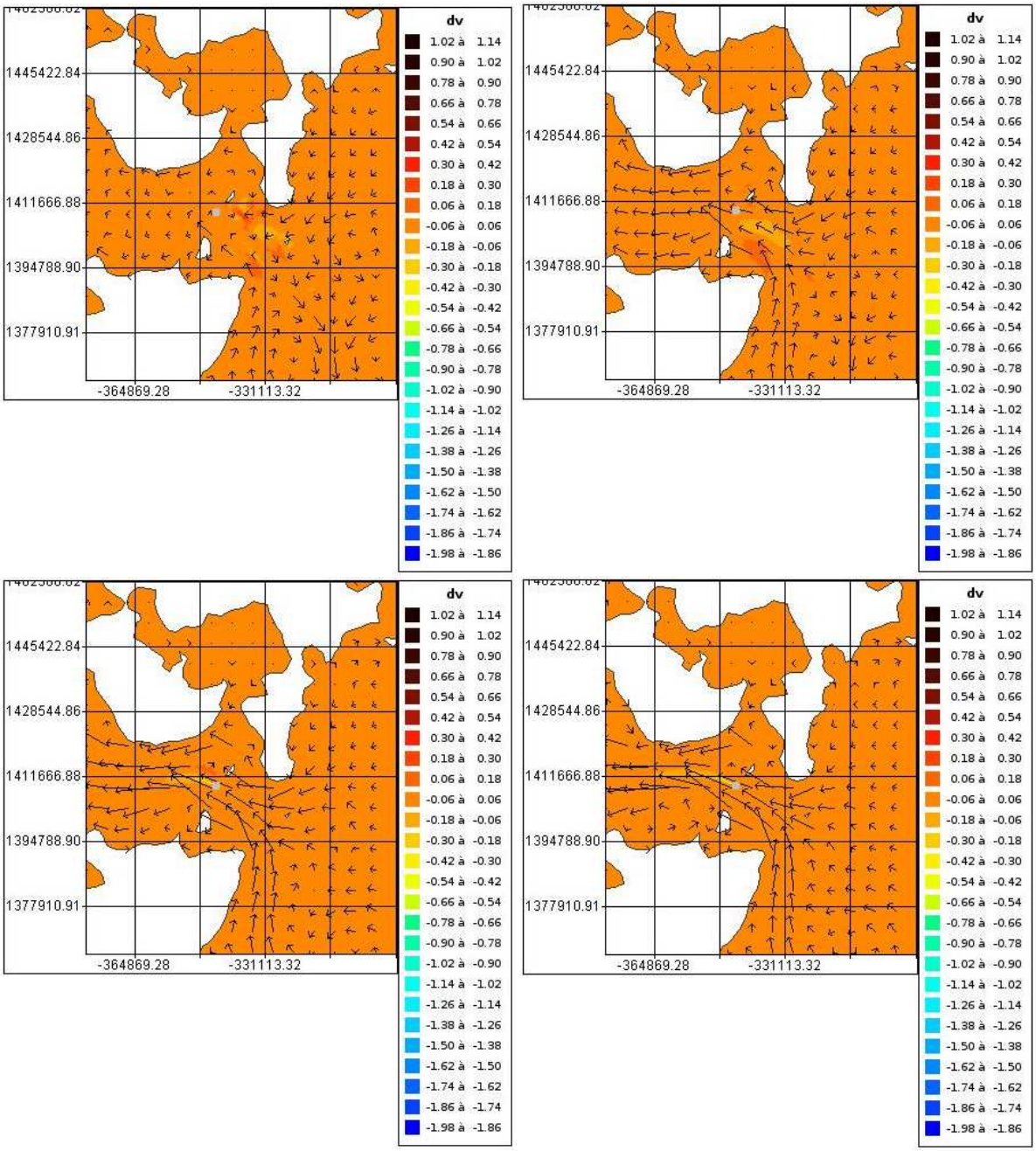
dv
1.02 à 1.14
0.90 à 1.02
0.78 à 0.90
0.66 à 0.78
0.54 à 0.66
0.42 à 0.54
0.30 à 0.42
0.18 à 0.30
0.06 à 0.18
-0.06 à 0.06
-0.18 à -0.06
-0.30 à -0.18
-0.42 à -0.30
-0.54 à -0.42
-0.66 à -0.54
-0.78 à -0.66
-0.90 à -0.78
-1.02 à -0.90
-1.14 à -1.02
-1.26 à -1.14
-1.38 à -1.26
-1.50 à -1.38
-1.62 à -1.50
-1.74 à -1.62
-1.86 à -1.74
-1.98 à -1.86
1445422.84
1428544.86
1411666.88
1394788.90
1377910.91
-364869.28
-331113.32

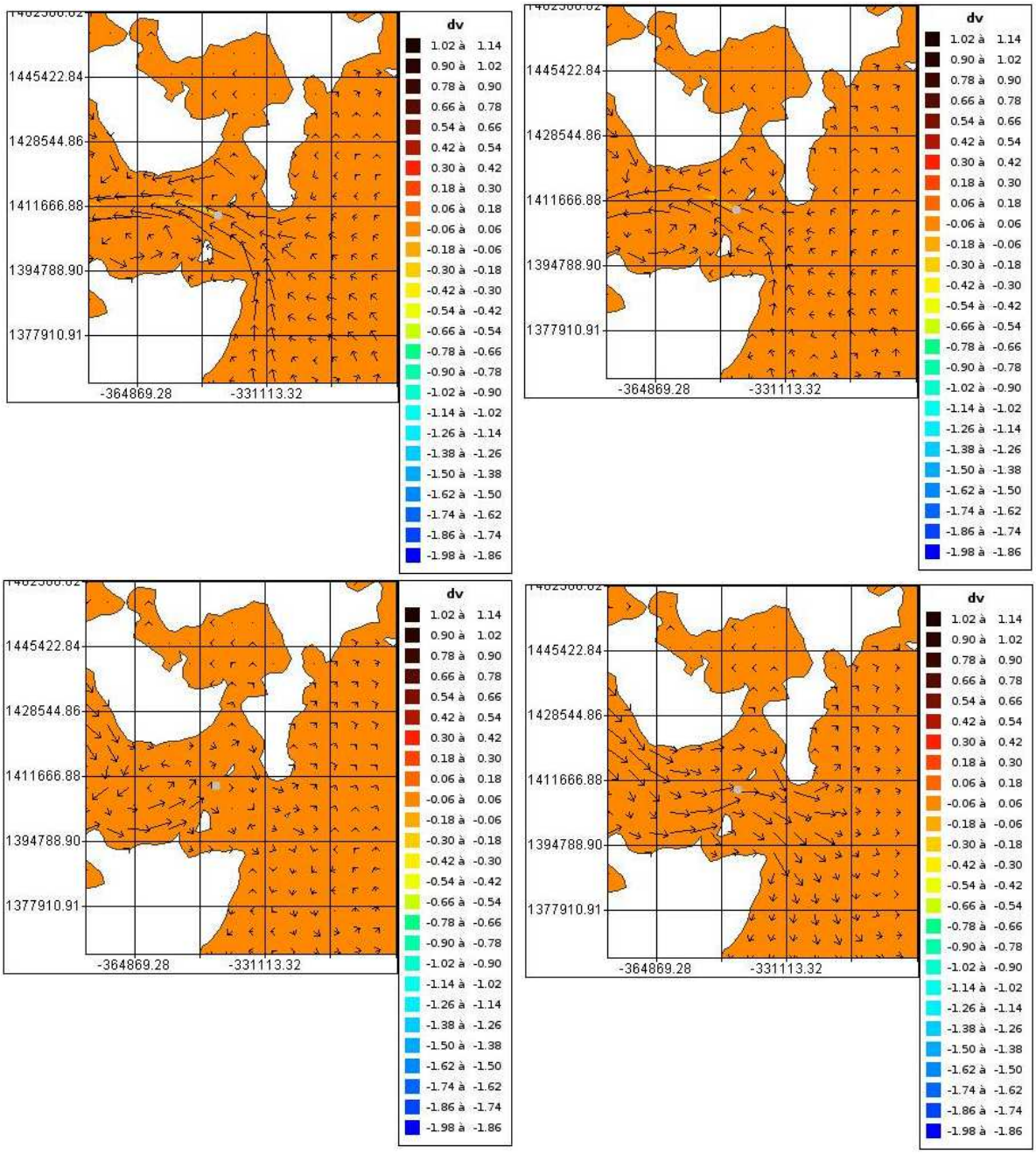
dv
1.02 à 1.14
0.90 à 1.02
0.78 à 0.90
0.66 à 0.78
0.54 à 0.66
0.42 à 0.54
0.30 à 0.42
0.18 à 0.30
0.06 à 0.18
-0.06 à 0.06
-0.18 à -0.06
-0.30 à -0.18
-0.42 à -0.30
-0.54 à -0.42
-0.66 à -0.54
-0.78 à -0.66
-0.90 à -0.78
-1.02 à -0.90
-1.14 à -1.02
-1.26 à -1.14
-1.38 à -1.26
-1.50 à -1.38
-1.62 à -1.50
-1.74 à -1.62
-1.86 à -1.74
-1.98 à -1.86
1445422.84
1428544.86
1411666.88
1394788.90
1377910.91
-364869.28
-331113.32

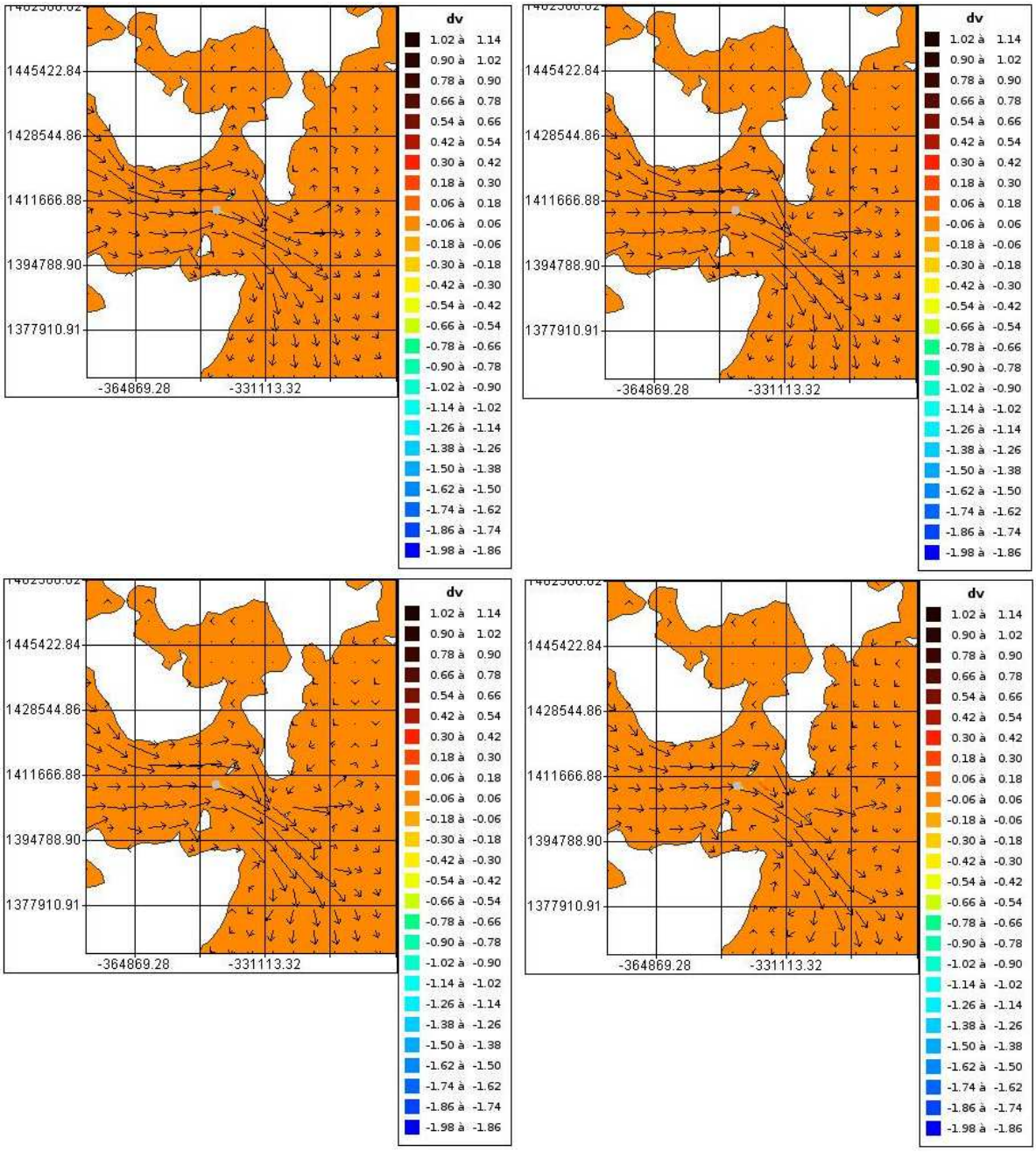
dv
1.02 à 1.14
0.90 à 1.02
0.78 à 0.90
0.66 à 0.78
0.54 à 0.66
0.42 à 0.54
0.30 à 0.42
0.18 à 0.30
0.06 à 0.18
-0.06 à 0.06
-0.18 à -0.06
-0.30 à -0.18
-0.42 à -0.30
-0.54 à -0.42
-0.66 à -0.54
-0.78 à -0.66
-0.90 à -0.78
-1.02 à -0.90
-1.14 à -1.02
-1.26 à -1.14
-1.38 à -1.26
-1.50 à -1.38
-1.62 à -1.50
-1.74 à -1.62
-1.86 à -1.74
-1.98 à -1.86
1445422.84
1428544.86
1411666.88
1394788.90
1377910.91
-364869.28
-331113.32

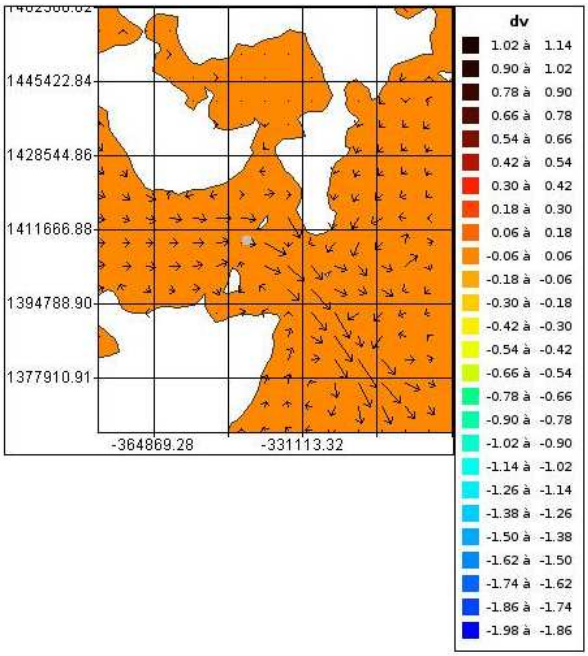

Figure 23: Hourly maps of the velocity difference dV (m/s) (dV = $V_{with\ TEC}$ - $V_{without\ TEC}$) and tidal velocity vectors of the flow simulated with turbines (black arrows). The gray shape is the tidal turbines.

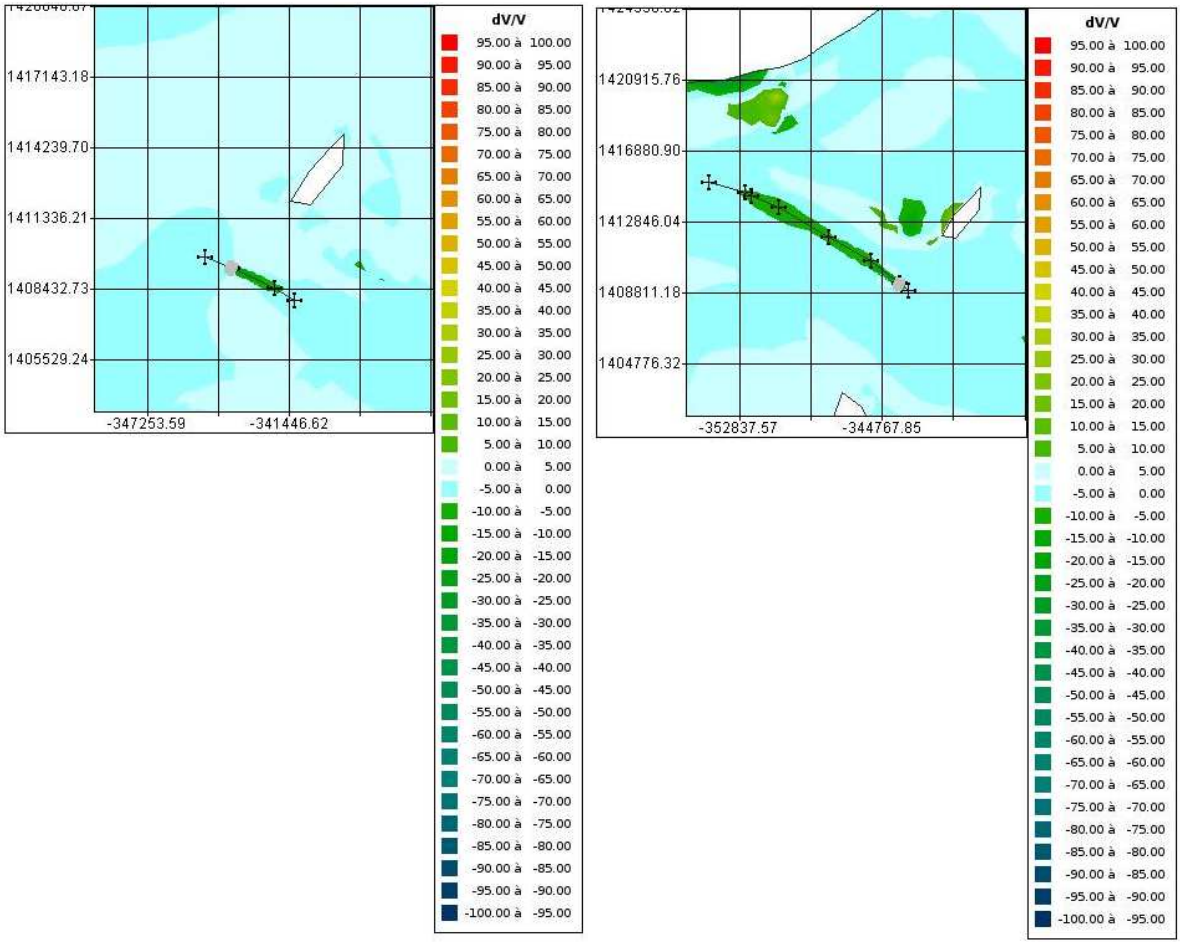

Figure 24: Location of the spatial profile during flood tide (left panel) and ebb tide (right panel).

It can be observed in Figure 24 that a much smaller disturbance is simulated during flood tide.

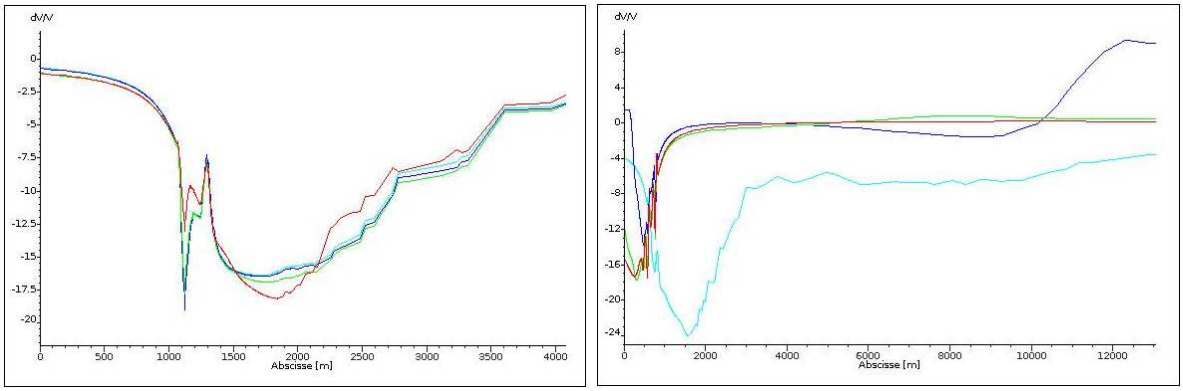

Figure 25: Reduction in tidal current speed along the wake of layout B tidal farm during flood (left panel) and ebb (right panel) tide. Line in light blue: maximum of tidal velocity (occurring at time h); blue line: tidal velocity at h+1 hour; green line: tidal velocity at h+2 hours; red line: tidal velocity at h+3 hours.

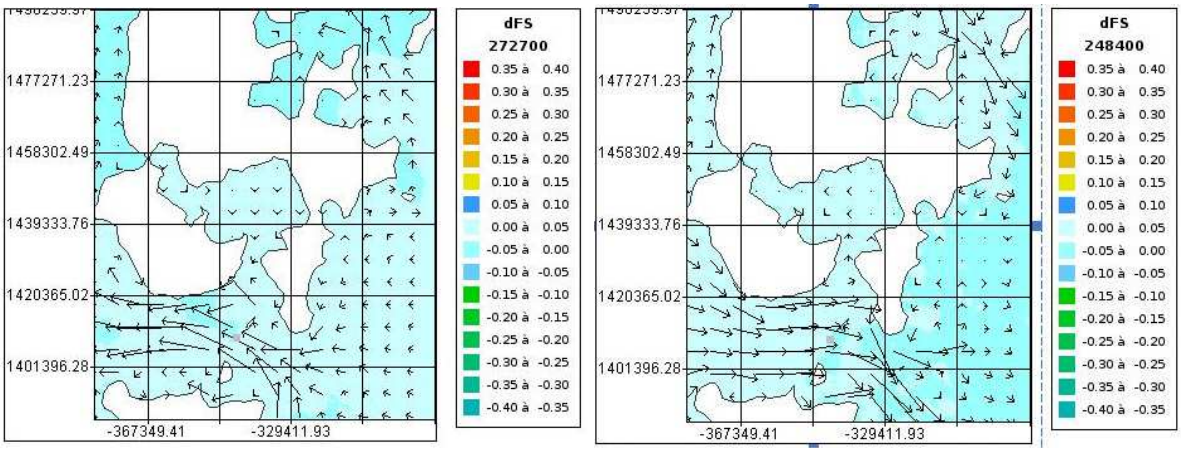

Figure 26: Differences in the free surface, during ebb (left panel) and flood tide (right panel). The gray line is the location of tidal turbines.

3.3.2.2.2 Neap tide

The main characteristics of the disturbances of the flow induced by the farm are the same as the ones as described in the previous section but with smaller effects. At ebb, wakes are around 5 km, as they are measured as the distance downstream until the velocity deficit becomes lower than 5 % of the unhindered flow conditions. During the flood, the wake is much smaller and around 2 km. Absolute velocity differences are much lower but the relative difference (expressed in %) along spatial profiles are similar (see Figure 27 and Figure 28).

Differences in the free surface elevations are also smaller with variations of maximal amplitude of +/- 0.05 m, see Figure 29.

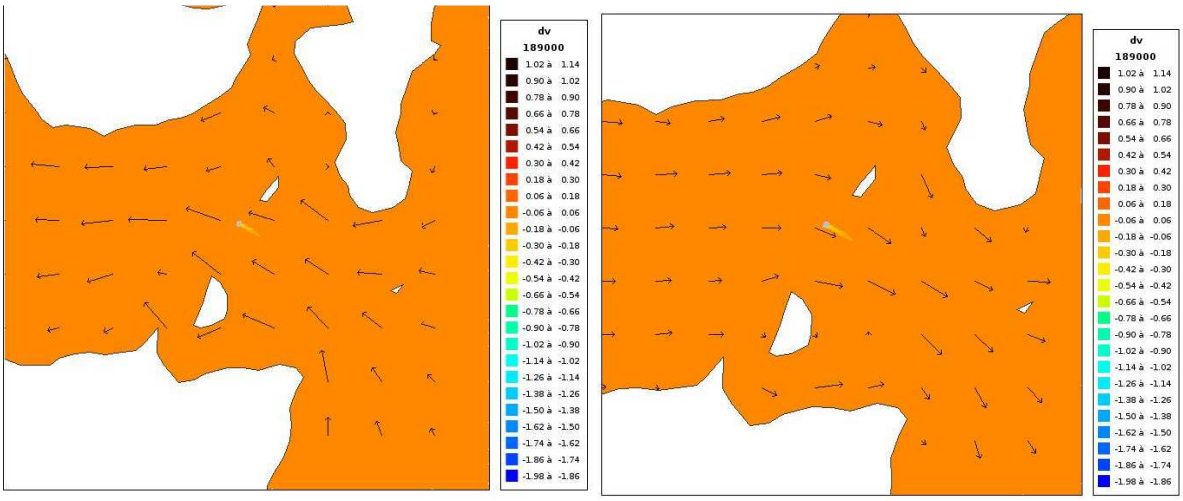

Figure 27: Wake downstream the tidal farm during the peak of ebb (left panel) and flood (right panel) of the neap tide.

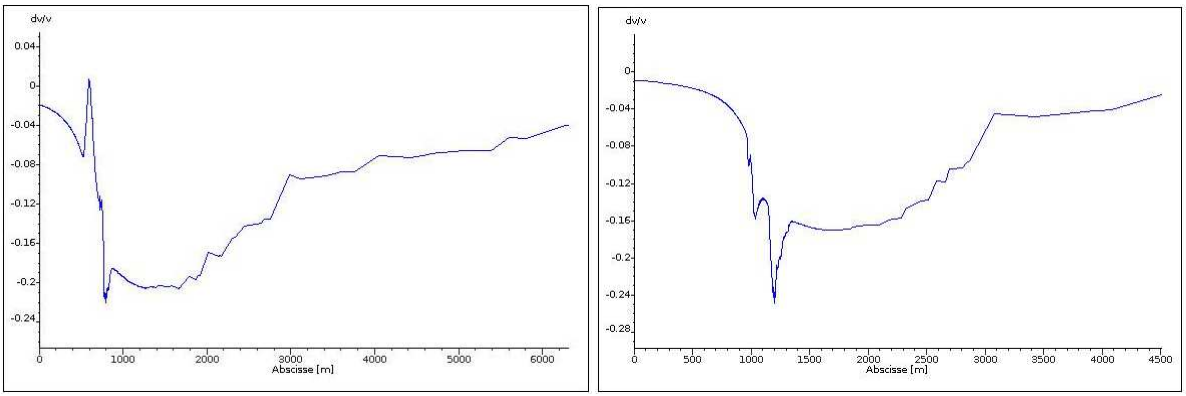

Figure 28: Evolution of tidal current velocity along the wake of layout B tidal farm during the ebb (left panel) and flood (right panel) tide. The red circle is located at the turbine location.

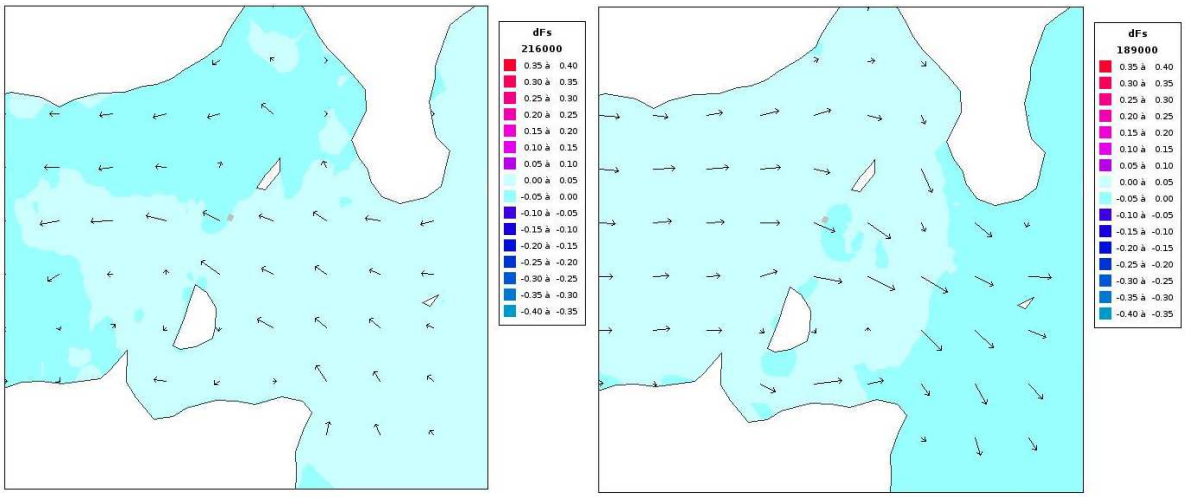

Figure 29: Difference in free surface, during ebb (left panel) and flood tide (right panel) - location of tidal turbines (gray line).

3.3.2.2.3 Power

This section describes the power evolution observed over the entire simulation. It can be observed in Figure 30 and Figure 31 that, around the 09/19, an anomalous peak of power occurred when the flow was simulated with linear elements. This reveals numerical instabilities of the simulation for a very short time. Figure 32 shows the comparison between the power evolution with and without the Quasi-Bubble option of Telemac-2D, where it can be observed that the anomalous peak of power has disappeared around the 09/19 with the Quasi-Bubble option.

The evolution of the tidal farm power (in W) follows the variations of the current intensity (see Figure 30) with highest power outputs during the spring tide and lowest power during the neap tide. However, fluid velocity fluctuations are dramatically amplified as power depends on the cube of the velocity.
The time-averaged power is roughly equal to 20 MW (equivalent to 0.71 MW/TEC). The power reaches a peak at 2.85 MW/TEC during spring tide to be compared to a "peak" power below 0.1 MW/TEC during the flood of the neap tide.

At last, we show in Figure 32 there are small differences in the mean power simulated with and without the "Quasi-Bubble" option. However as this option allows erroneous power estimates, it gives better estimates of the current power evolution.

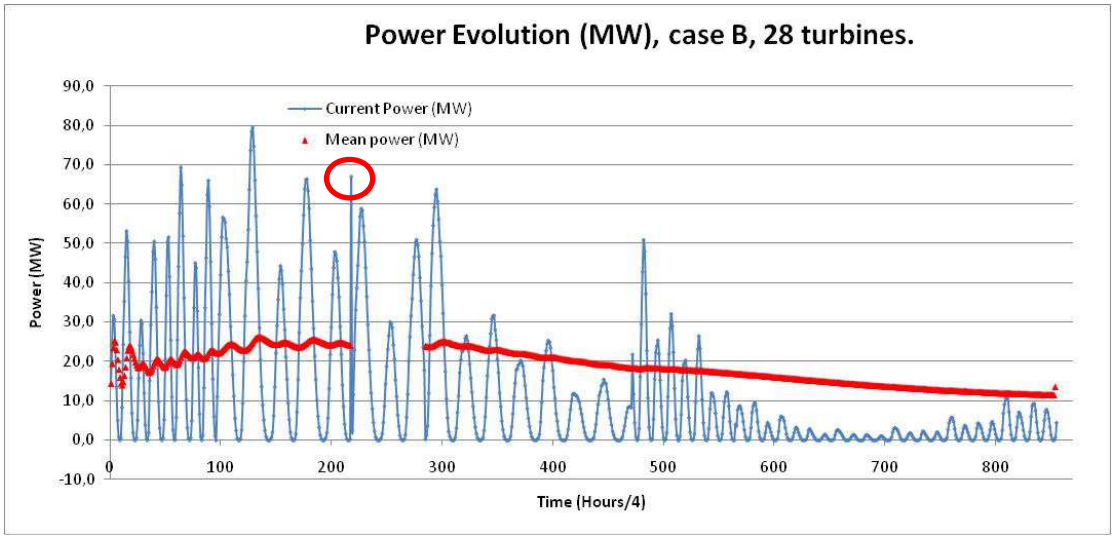

Figure 30: Current and mean power evolution for case B. The abnormal pick of power is surrounded by the red circle.

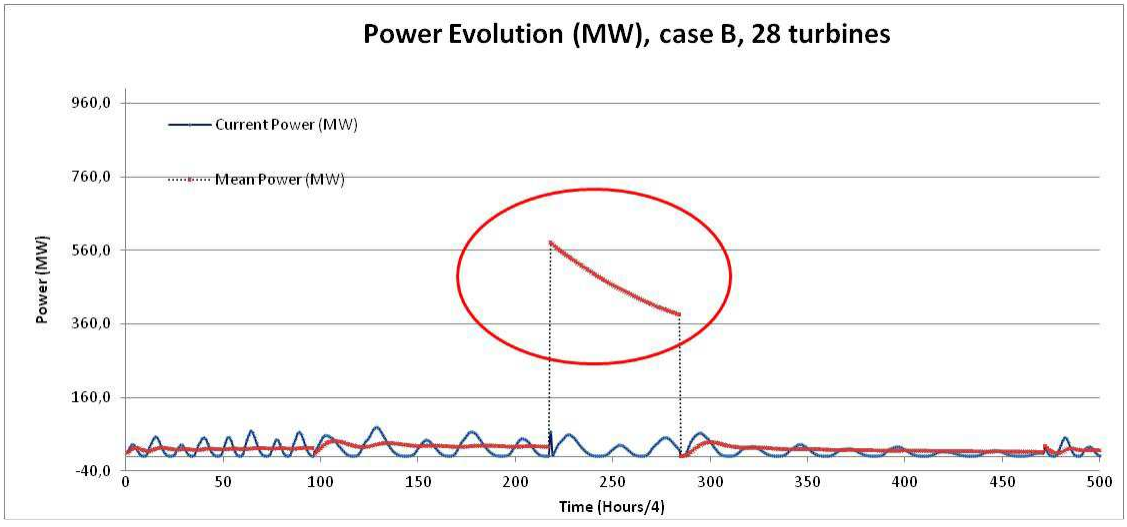

Figure 31: Current and Mean power anomaly around the 09/19.

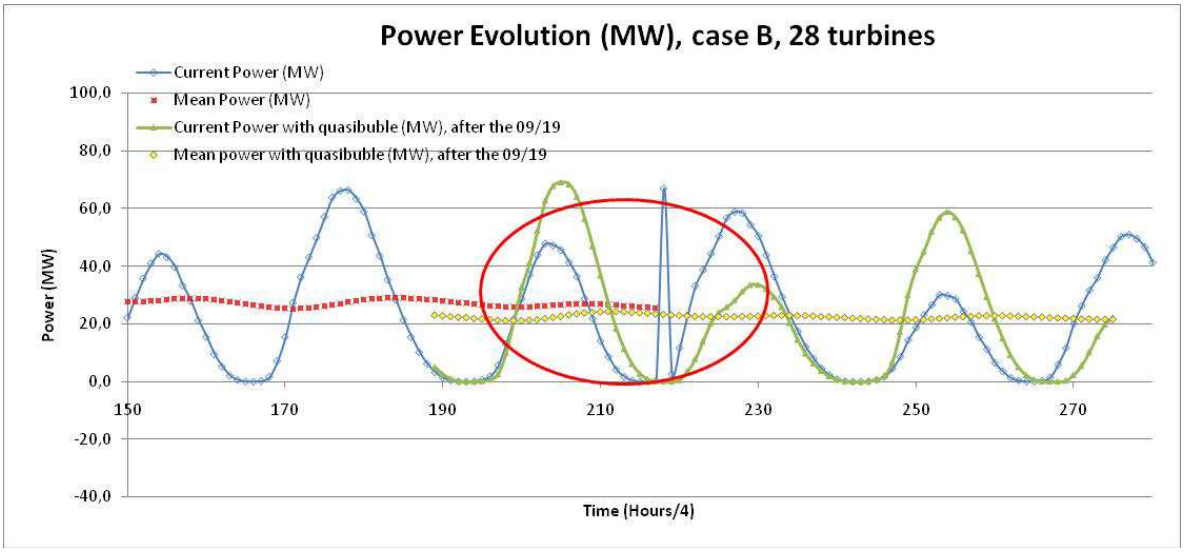

Figure 32: Comparison of the power evolution (mean and current) around the 09/19 with or without the Quasi-Bubble option of Telemac-2D. With the Quasi-Bubble option, no abnormal pick of power is observed.

3.3.3 Tidal farm layout C

The turbines are represented by a single global box using the DRAGFO routine of Telemac-2D following the global box method (see [A3]). The flow is examined in details during the spring tide identified in the previous section and the main features are analysed during the neap tide.

3.3.3.1 Global Box

The array of 250 turbines are modelled according to the Global Box methodology as explained in WG3 WP3 D3 (cf. [A3] § 2.3). All turbines are individually modelled in a rectangular flume (whose dimensions are roughly about 1750 m x 8000 m), see Figure 33 and Figure 34.

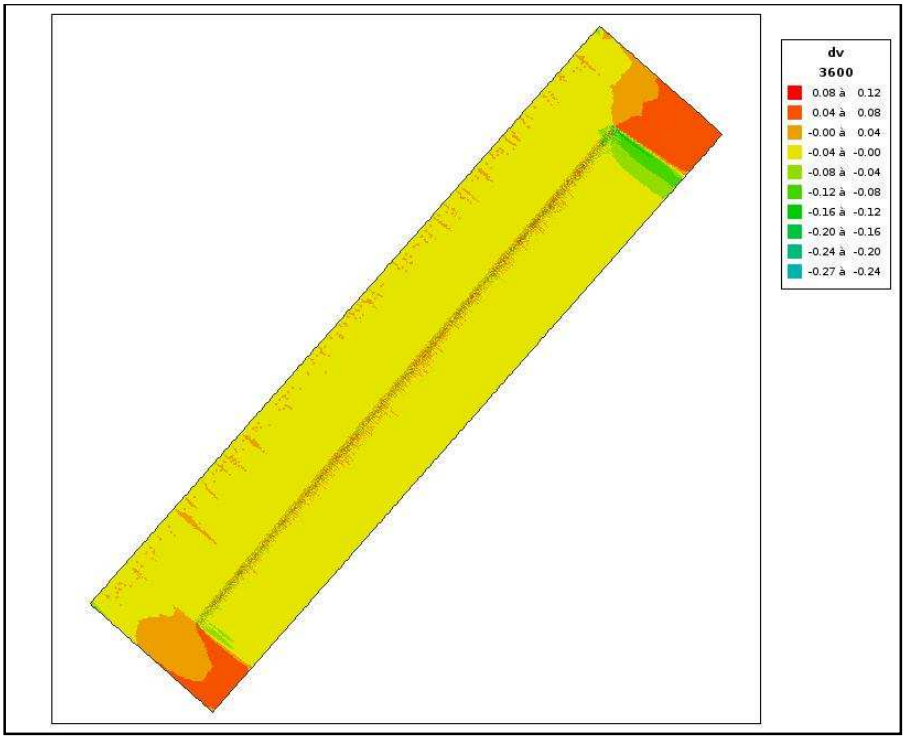

Figure 33: Velocity deficit observed with Layout C inside the global box.

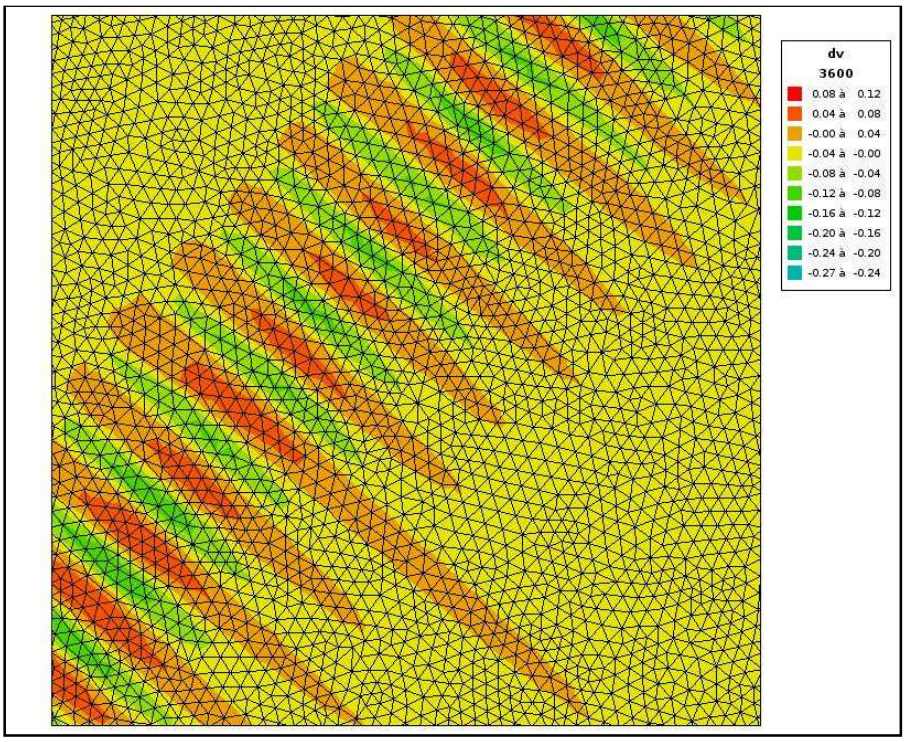

Figure 34: Zoom of the velocity deficit observed with Layout A inside the global box.

Along the stream direction, the arrays are at least 800 m away from the boundary, corresponding to a distance of 45*D*, where *D* is the turbine diameter (here 18 m). Perpendicular to the stream direction, turbines are at a minimal distance of 660 m, i.e. 36*D* from the walls. The bathymetry of the canal is idealised. The bathymetry is homogeneously flat at a depth of 70 m. The inflow is imposed at a 2.0

m/s speed (a typical mean velocity near the Pentland Firth) and defines the upstream reference velocity.

The energy is then integrated throughout transversal sections of the canal. The obtained results are provided in Figure 35. The power variations (in MW) are indicated all along the longitudinal axis of the domain (blue curve). The energy loss solely due to the turbine action is derived from this curve by identifying the deficit of energy near the turbines location: Just upstream and downstream the gap, we localize points representing the middle of the oscillations of the power. Then, dE/dt is the difference between the values of those two points.

The resulting energy loss is estimated at 250 MW resulting in an equivalent drag coefficient Cd of 0.88 for the 250-turbine tidal farm by applying equation (8) of WG3WP3 D3 (cf. [A3] § 2.3).

The tidal farm is then modelled in Telemac-2D by applying the equivalent drag force in the area of a global box using the routine DRAGFO (see [A3] for more details).

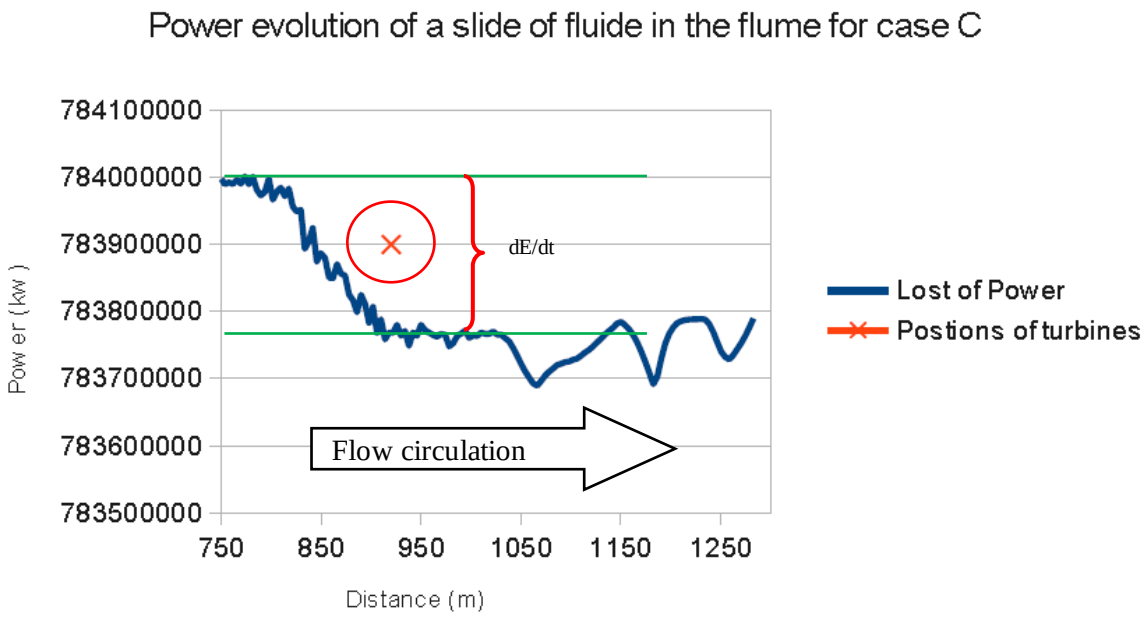

Figure 35: Variation of power (MW) near the turbines location throughout the longitudinal axis of the global box domain (Blue curve). The circle surrounds the area where the turbines are located.

3.3.3.2 Impact of tidal farm C

3.3.3.2.1 Spring tide

The evolution of the perturbations induced by the tidal farm during the spring tide is illustrated by a series of hourly maps of the velocity difference, dV (m/s), between simulations with and without turbines ($dV = V_{with\ TEC} - V_{without\ TEC}$), displayed with the velocity vectors of the flow simulation accounting for turbines, see Figure 36.

The hydrodynamics effects of the tidal energy extraction results in the development of a wake downstream the farm which interacts with the surrounding islands and the coast. This means that the shape and size of the wake can be sometimes not clearly identified. Moreover, Figure 39 shows that tidal velocities are reduced near the turbine location by roughly 10%. When expressed in %, dV is calculated as follows: $dV = (V_{with\ TEC} - V_{without\ TEC}) / V_{without\ TEC}$. Significant velocity reductions (dV > 5

%) are experienced downstream of the farm throughout roughly 40 km during the peak of ebb of the spring tide. The impact is also characterised by some disturbance of the flow in the surroundings, see Figure 37 and Figure 38.

Moreover, the free surface (FS) is also impacted but the effects of the farm remains relatively low. The surface decreases downstream the farm and increases upstream (see Figure 41 and Figure 42). The maximal variations of free surface elevation are localised close to the farm and their amplitude are of the order of +/- 5-10 cm compared to the initial state.

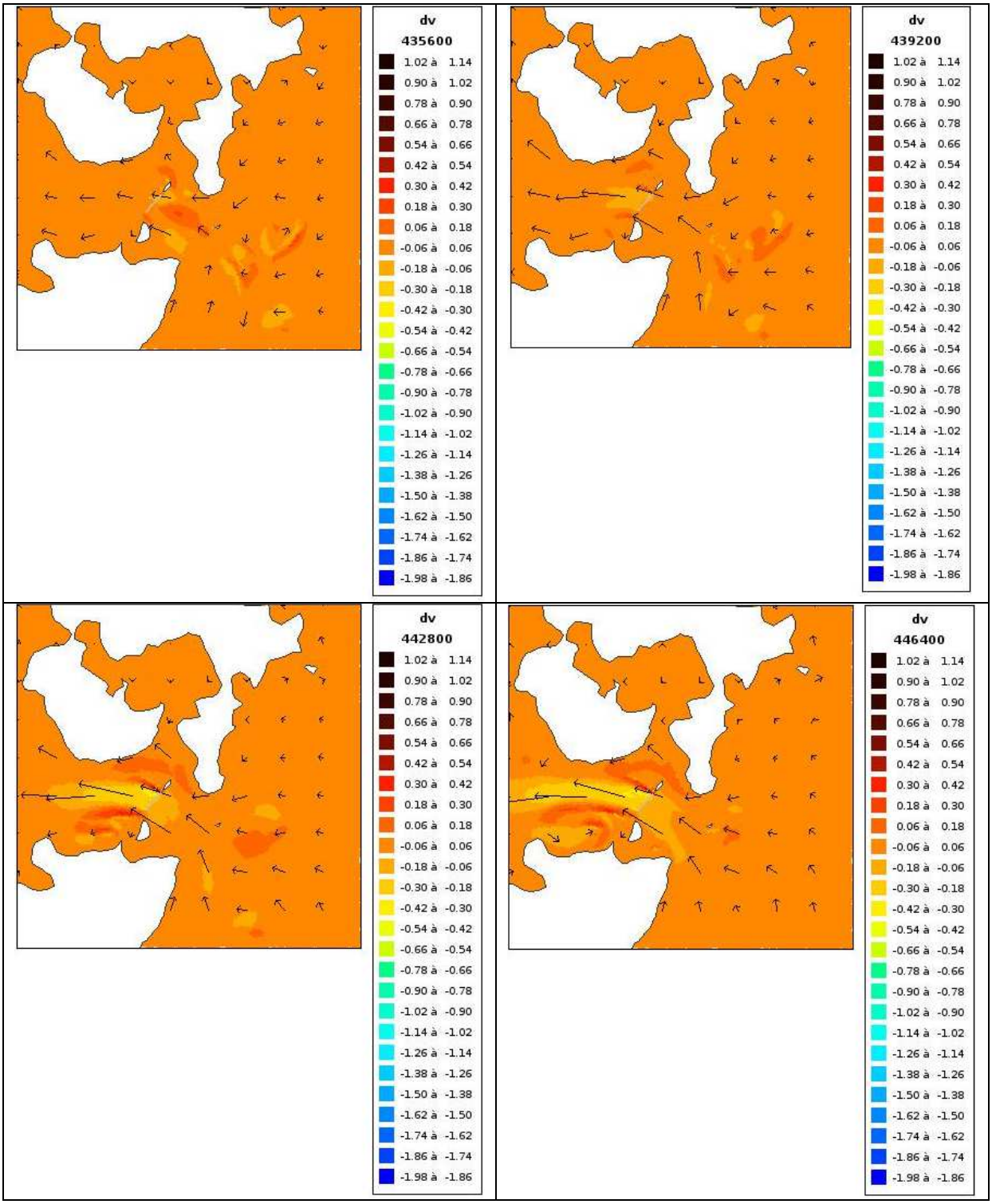

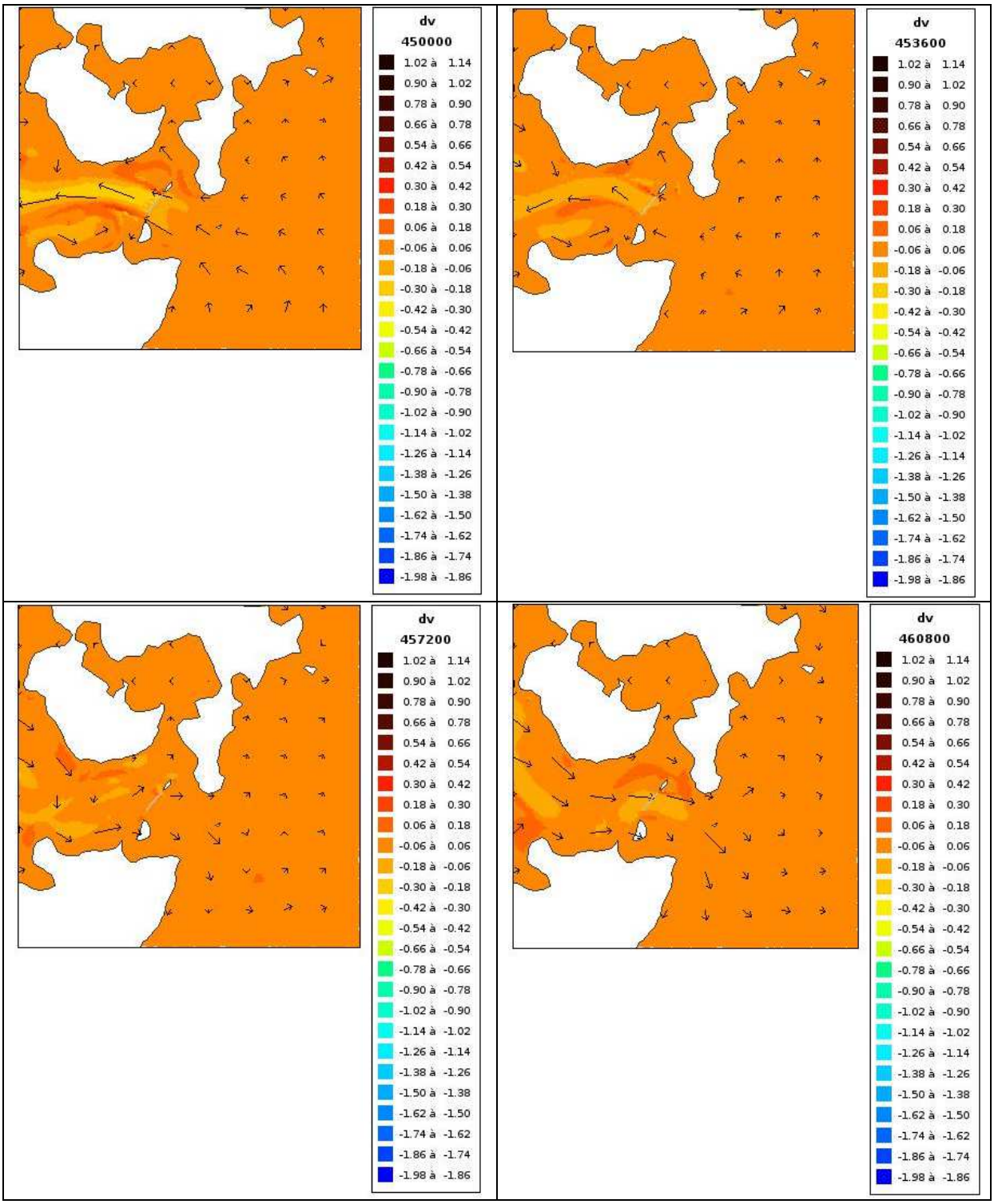
dv
450000
1.02 à 1.14
0.90 à 1.02
0.78 à 0.90
0.66 à 0.78
0.54 à 0.66
0.42 à 0.54
0.30 à 0.42
0.18 à 0.30
0.06 à 0.18
-0.06 à 0.06
-0.18 à -0.06
-0.30 à -0.18
-0.42 à -0.30
-0.54 à -0.42
-0.66 à -0.54
-0.78 à -0.66
-0.90 à -0.78
-1.02 à -0.90
-1.14 à -1.02
-1.26 à -1.14
-1.38 à -1.26
-1.50 à -1.38
-1.62 à -1.50
-1.74 à -1.62
-1.86 à -1.74
-1.98 à -1.86
dv
453600
1.02 à 1.14
0.90 à 1.02
0.78 à 0.90
0.66 à 0.78
0.54 à 0.66
0.42 à 0.54
0.30 à 0.42
0.18 à 0.30
0.06 à 0.18
-0.06 à 0.06
-0.18 à -0.06
-0.30 à -0.18
-0.42 à -0.30
-0.54 à -0.42
-0.66 à -0.54
-0.78 à -0.66
-0.90 à -0.78
-1.02 à -0.90
-1.14 à -1.02
-1.26 à -1.14
-1.38 à -1.26
-1.50 à -1.38
-1.62 à -1.50
-1.74 à -1.62
-1.86 à -1.74
-1.98 à -1.86
dv
457200
1.02 à 1.14
0.90 à 1.02
0.78 à 0.90
0.66 à 0.78
0.54 à 0.66
0.42 à 0.54
0.30 à 0.42
0.18 à 0.30
0.06 à 0.18
-0.06 à 0.06
-0.18 à -0.06
-0.30 à -0.18
-0.42 à -0.30
-0.54 à -0.42
-0.66 à -0.54
-0.78 à -0.66
-0.90 à -0.78
-1.02 à -0.90
-1.14 à -1.02
-1.26 à -1.14
-1.38 à -1.26
-1.50 à -1.38
-1.62 à -1.50
-1.74 à -1.62
-1.86 à -1.74
-1.98 à -1.86
dv
460800
1.02 à 1.14
0.90 à 1.02
0.78 à 0.90
0.66 à 0.78
0.54 à 0.66
0.42 à 0.54
0.30 à 0.42
0.18 à 0.30
0.06 à 0.18
-0.06 à 0.06
-0.18 à -0.06
-0.30 à -0.18
-0.42 à -0.30
-0.54 à -0.42
-0.66 à -0.54
-0.78 à -0.66
-0.90 à -0.78
-1.02 à -0.90
-1.14 à -1.02
-1.26 à -1.14
-1.38 à -1.26
-1.50 à -1.38
-1.62 à -1.50
-1.74 à -1.62
-1.86 à -1.74
-1.98 à -1.86

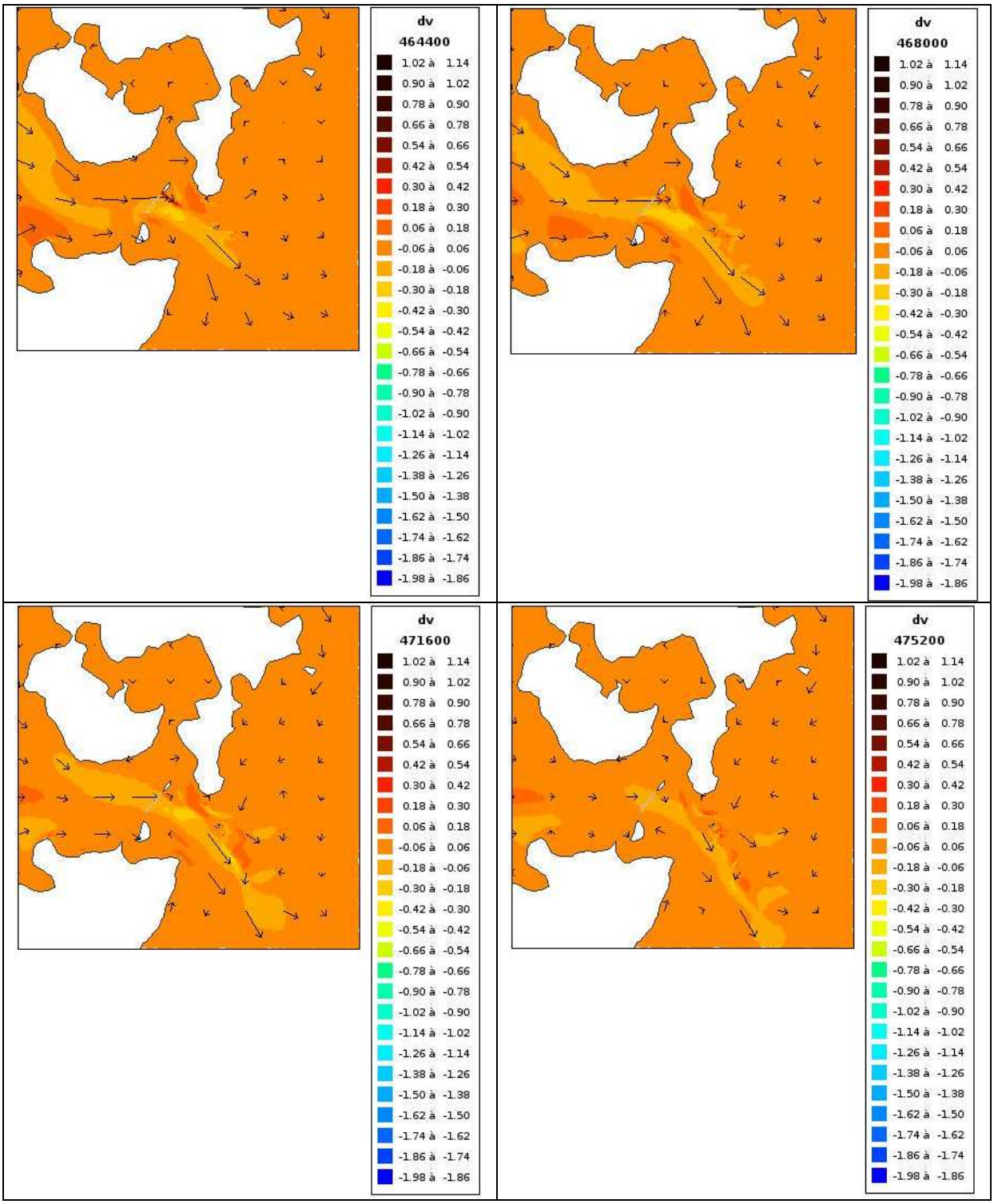
dv
464400
1.02 à 1.14
0.90 à 1.02
0.78 à 0.90
0.66 à 0.78
0.54 à 0.66
0.42 à 0.54
0.30 à 0.42
0.18 à 0.30
0.06 à 0.18
-0.06 à 0.06
-0.18 à -0.06
-0.30 à -0.18
-0.42 à -0.30
-0.54 à -0.42
-0.66 à -0.54
-0.78 à -0.66
-0.90 à -0.78
-1.02 à -0.90
-1.14 à -1.02
-1.26 à -1.14
-1.38 à -1.26
-1.50 à -1.38
-1.62 à -1.50
-1.74 à -1.62
-1.86 à -1.74
-1.98 à -1.86
dv
468000
1.02 à 1.14
0.90 à 1.02
0.78 à 0.90
0.66 à 0.78
0.54 à 0.66
0.42 à 0.54
0.30 à 0.42
0.18 à 0.30
0.06 à 0.18
-0.06 à 0.06
-0.18 à -0.06
-0.30 à -0.18
-0.42 à -0.30
-0.54 à -0.42
-0.66 à -0.54
-0.78 à -0.66
-0.90 à -0.78
-1.02 à -0.90
-1.14 à -1.02
-1.26 à -1.14
-1.38 à -1.26
-1.50 à -1.38
-1.62 à -1.50
-1.74 à -1.62
-1.86 à -1.74
-1.98 à -1.86
dv
471600
1.02 à 1.14
0.90 à 1.02
0.78 à 0.90
0.66 à 0.78
0.54 à 0.66
0.42 à 0.54
0.30 à 0.42
0.18 à 0.30
0.06 à 0.18
-0.06 à 0.06
-0.18 à -0.06
-0.30 à -0.18
-0.42 à -0.30
-0.54 à -0.42
-0.66 à -0.54
-0.78 à -0.66
-0.90 à -0.78
-1.02 à -0.90
-1.14 à -1.02
-1.26 à -1.14
-1.38 à -1.26
-1.50 à -1.38
-1.62 à -1.50
-1.74 à -1.62
-1.86 à -1.74
-1.98 à -1.86
dv
475200
1.02 à 1.14
0.90 à 1.02
0.78 à 0.90
0.66 à 0.78
0.54 à 0.66
0.42 à 0.54
0.30 à 0.42
0.18 à 0.30
0.06 à 0.18
-0.06 à 0.06
-0.18 à -0.06
-0.30 à -0.18
-0.42 à -0.30
-0.54 à -0.42
-0.66 à -0.54
-0.78 à -0.66
-0.90 à -0.78
-1.02 à -0.90
-1.14 à -1.02
-1.26 à -1.14
-1.38 à -1.26
-1.50 à -1.38
-1.62 à -1.50
-1.74 à -1.62
-1.86 à -1.74
-1.98 à -1.86

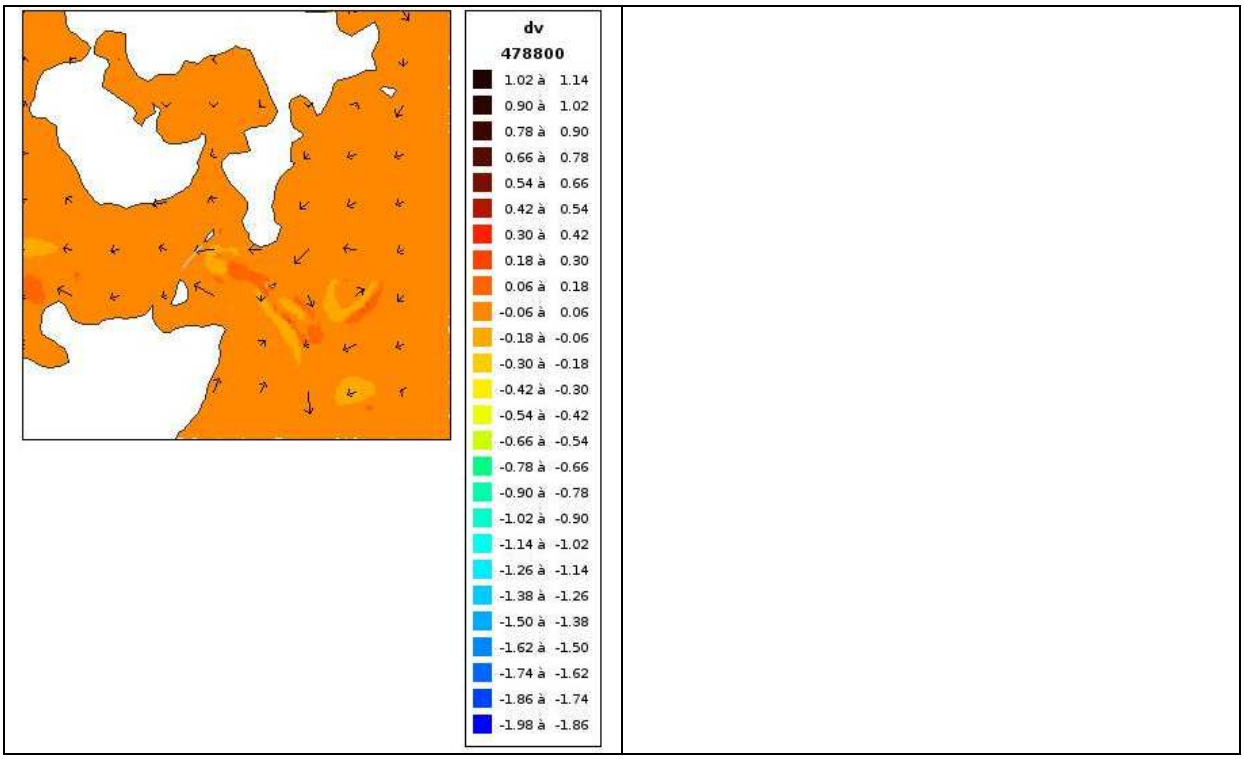

Figure 36: Hourly maps of the velocity differences dV (m/s) (dV = $V_{\text{with TEC}}$ - $V_{\text{without TEC}}$) and tidal velocity vectors of the flow simulated with turbines (black arrows). The gray shape is the tidal turbines.

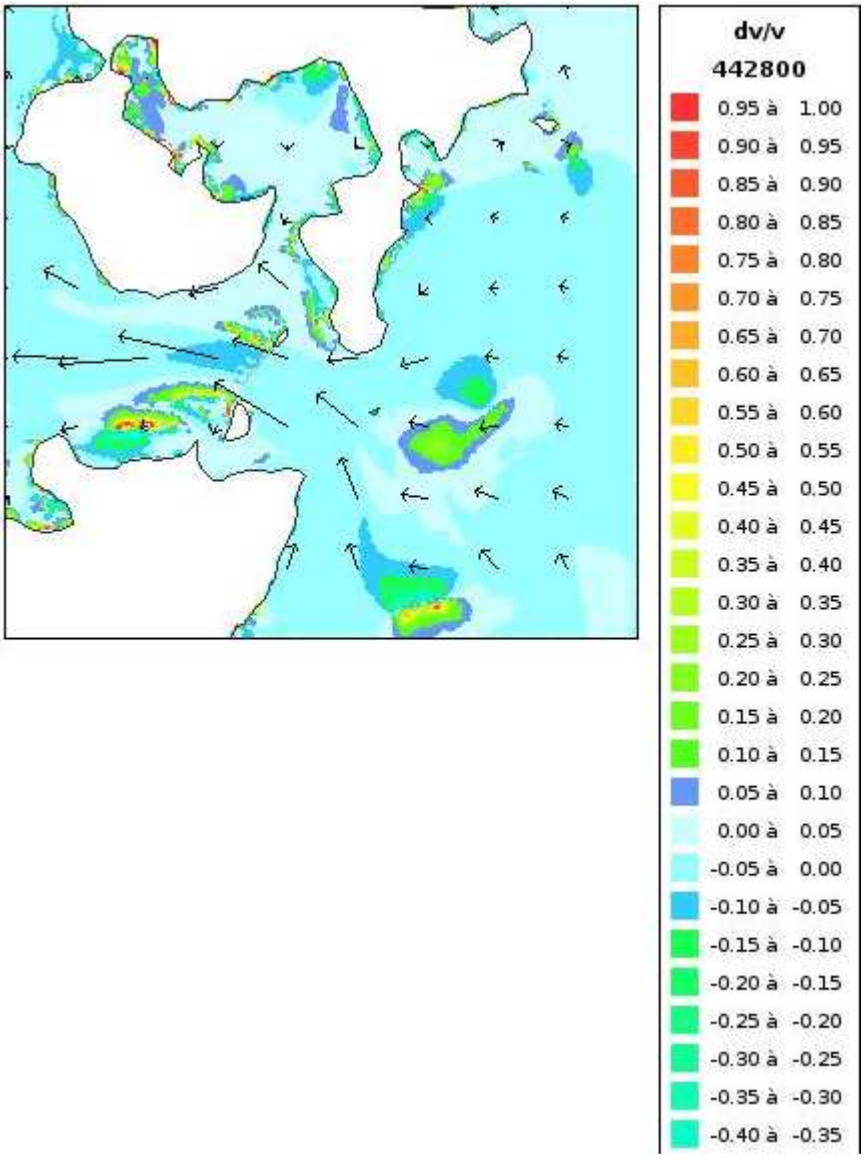

Figure 37: Relative variation of the velocity observed when the current velocity (at low tide) is maximal. The gray shape is the tidal turbines.

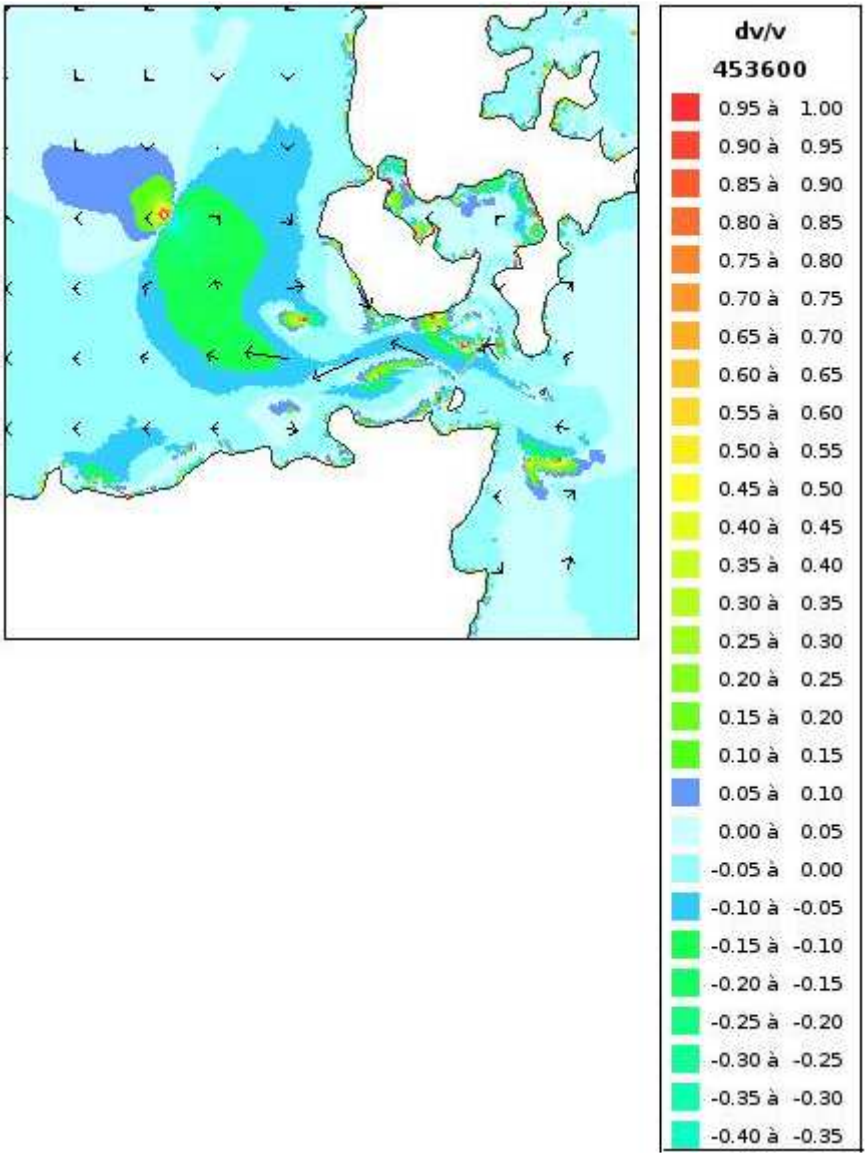

Figure 38: Relative variation of the velocity. Maximum wake length observed 3 hours after the maximal current velocity (at low tide). The gray shape is the tidal turbines.

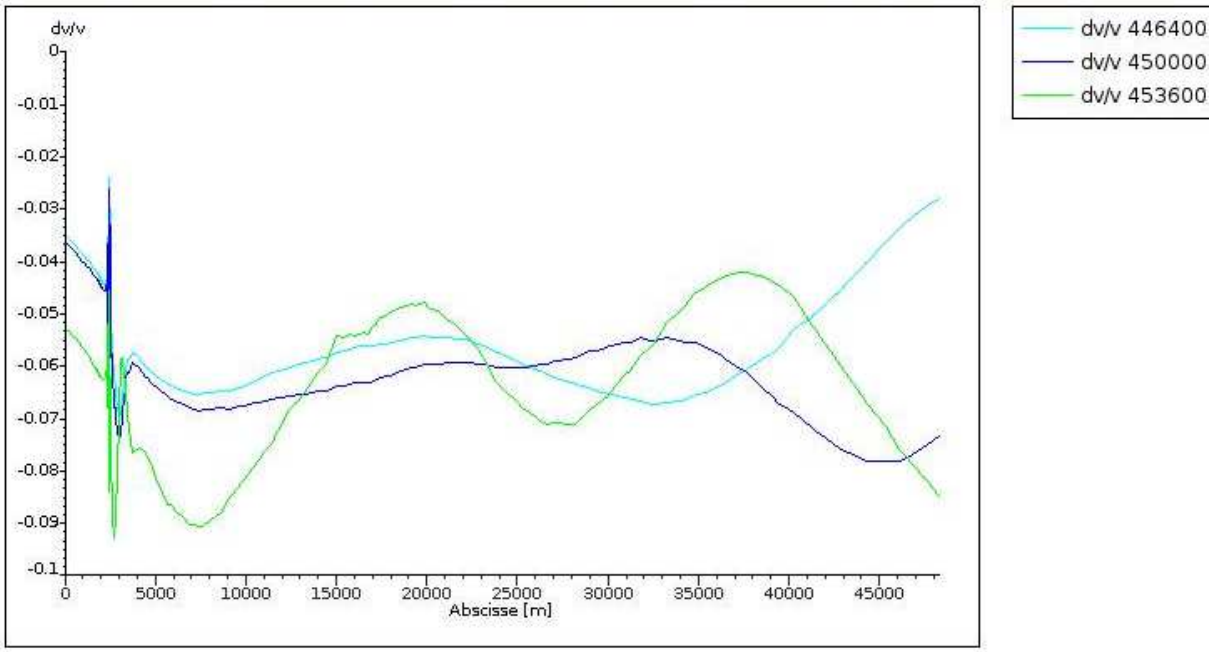

Figure 39: Reduction in tidal current velocity along the wake of tidal farm layout A at low tide. Line in light blue: maximum of tidal velocity (occurring at time h); blue line: tidal velocity at h+1 hour; green line: tidal velocity at h+2 hours.

In Figure 39, the distance from the turbine where the velocity is equal to 95% of the initial velocity is about 40 km. The row of turbine is 3.6 km long, and then the wake is roughly equal to 11x(length of the row turbines).

Figure 40 shows the difficulties to evaluate the wake just after the high tide. The presence of the surrounding islands and the coast explains the observed perturbations. For example, the wake is drawn in Figure 40 one hour after the high tide:

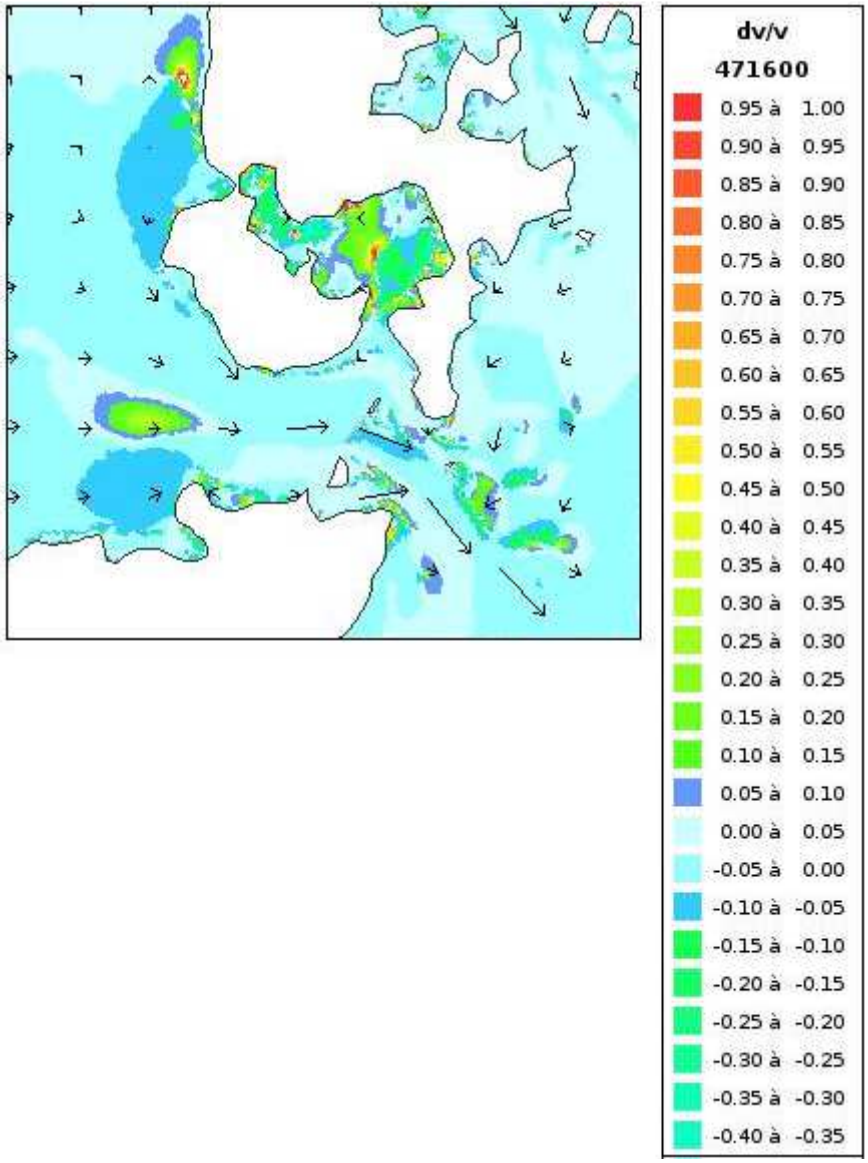

Figure 40: Wake observed 1 hour after the high tide. The gray shape is the tidal turbines.

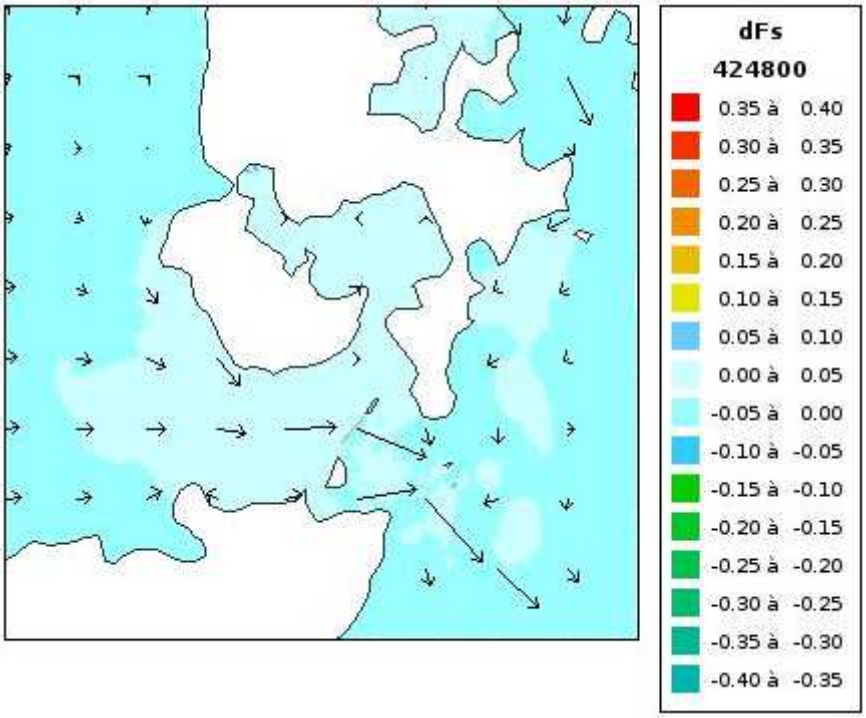

Figure 41: Differences in free surface, dFS (m), during flood (one hour after the maximal velocity) - location of tidal turbines (gray line).

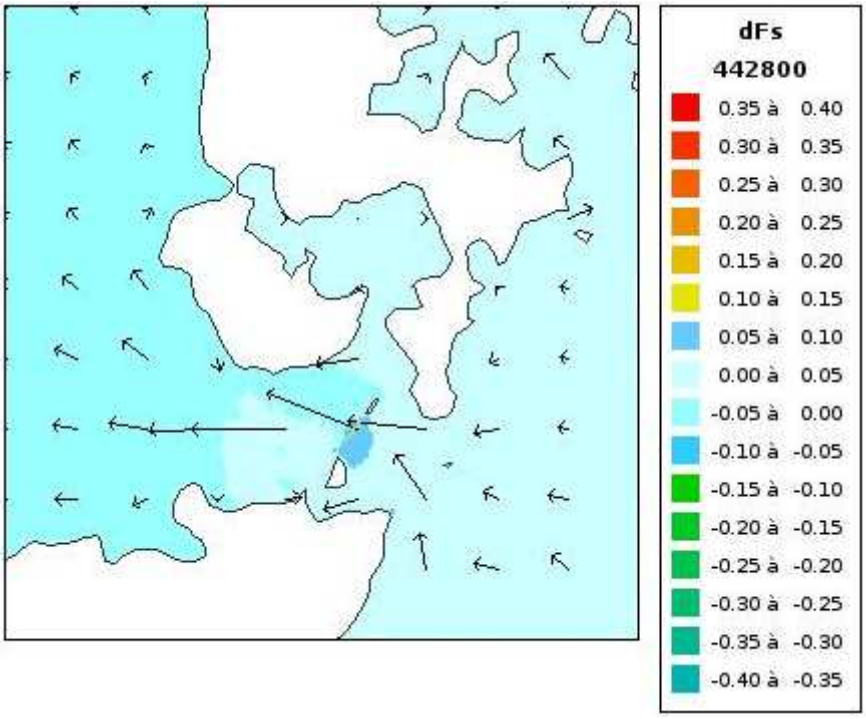

Figure 42: Differences in free surface, dFS (m), during ebb (at the maximal velocity) - location of tidal turbines (gray line).

One would have expected a bigger wake for this case C because of the size of the farm. Differences in the observed wake between case A and case C can be explained by the fact that, first, the number of turbines is different, and second, the equivalent drag coefficients are not the same (1.01 for case A and 0.88 for case C). So, the difference between the drag coefficients used is about 15% which has an impact on the flow.
Moreover, the difference in the observed wake between case C and case B can be explained by the fact that, first, the number of turbines is different, and second, the number of rows is not the same: 2 drag forces have an impact on the velocity for case B (it is as if there were 2 drag coefficients for case B, or one drag equal to nearly twice the value of the drag coefficient of case C), and for case C, only one drag force has an action. Those differences have different impact on the flow. Therefore, even if we can expect for case C to observe the most important wake, due to the special features of the tidal farm A, B and C, this does not appear in fact. The same observation can be made at neap tide.

3.3.3.2.2 Neap tide

The main characteristics of the disturbances of the flow induced by the farm are the same as the ones described in the previous section. During the ebb and the flood, the wake is much smaller.

Differences in free surface elevations are also smaller with variations of maximal amplitude of +/- 0.05 m.

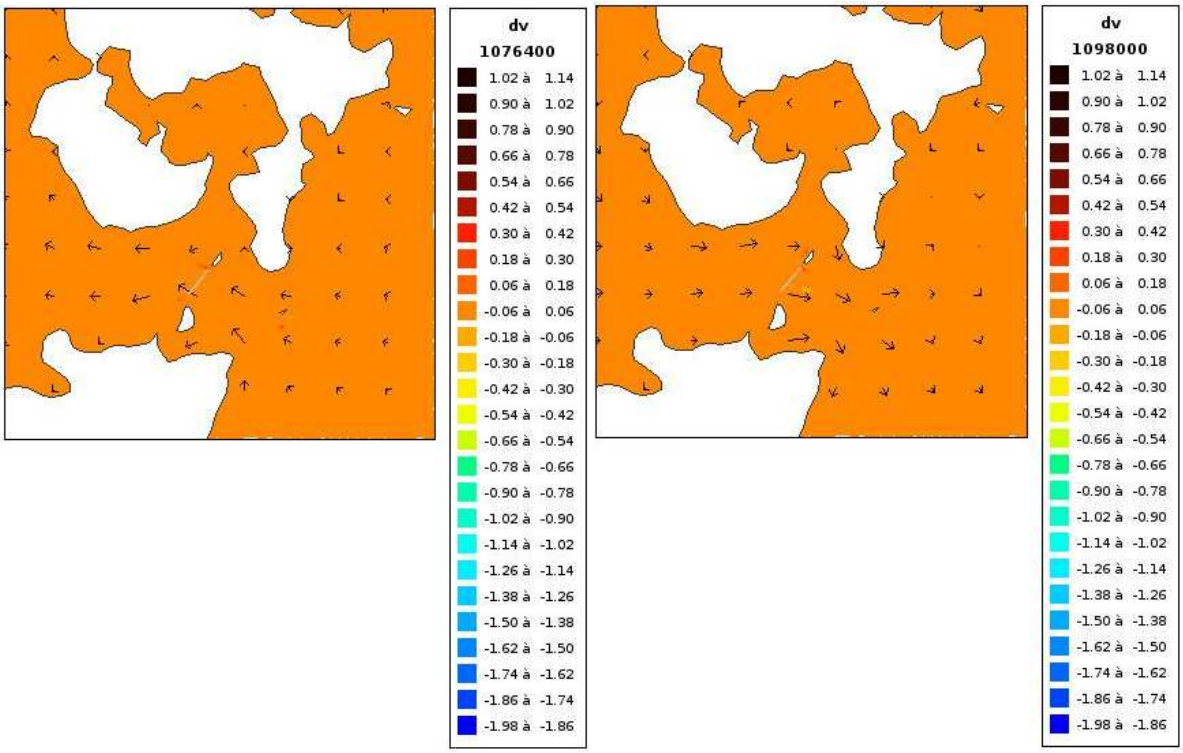

Figure 43: Wake downstream the tidal farm during the peak of ebb (left panel) and flood (right panel) of the neap tide.

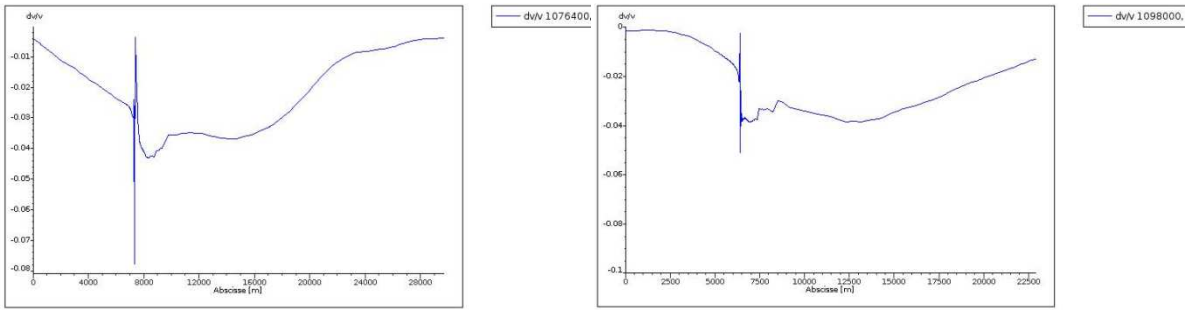

Figure 44: Evolution of tidal current velocity along the wake of layout A tidal farm during the ebb (left panel) and flood (right panel) tide. The red circle is located at the turbine location.

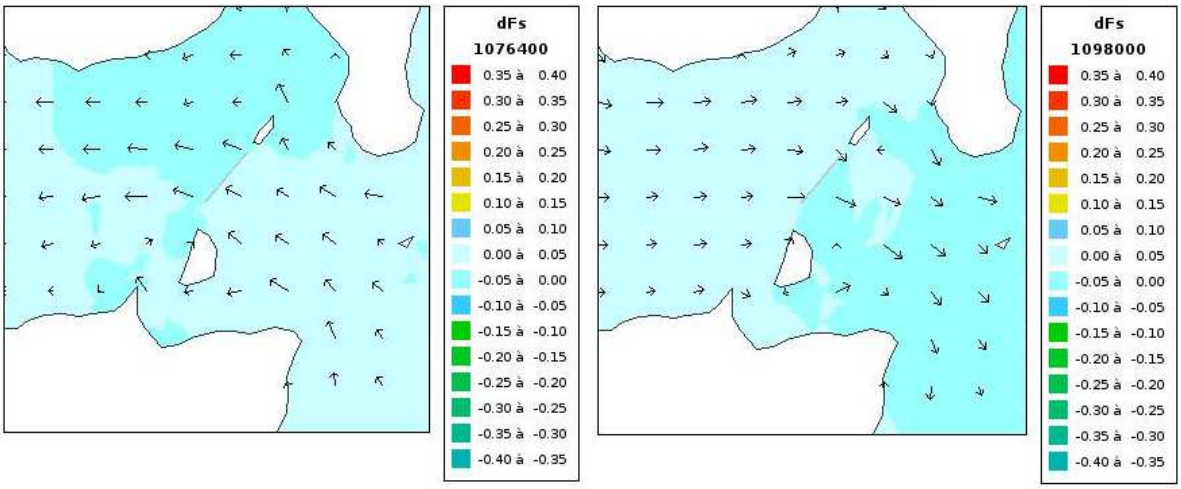

Figure 45: Difference in free surface, during ebb (left panel) and flood tide (right panel) - location of tidal turbines (gray line).

3.3.3.2.3 Power

This section describes the power evolution observed with the “Quasi-Bubble” option set in Telemac-2D in case C. The power evolution is presented in Figure 46.

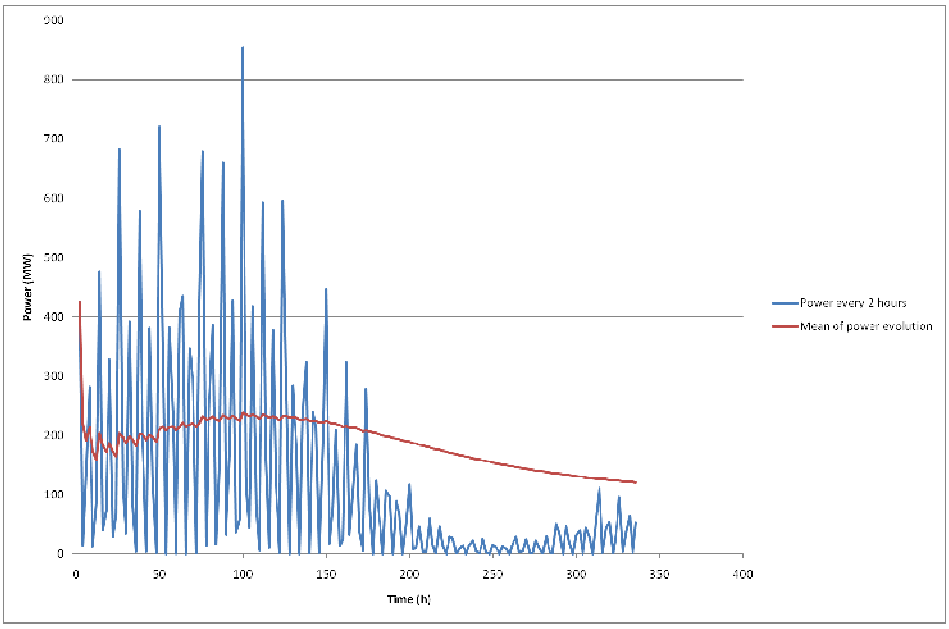

Figure 46: Mean and current power evolution for case C.

The time-averaged power is roughly equal to 190 MW (equivalent to 0.75 MW/TEC). The power reaches a peak at 3.4 MW/TEC during spring tide, which should be compared to a "peak" power below 0.12 MW/TEC during the flood of the neap tide.

3.4 Concluding remarks

The first concluding remark is that to model large farms at such a large scale quasi-bubble elements need to be used to model the flow velocities. This reduces greatly numerical instabilities which can produce erroneous flow velocities for short periods of time. This therefore allows the impact of the turbines in relation to the unhindered flow to be assessed. Furthermore, as the fluid velocities are better modelled instantaneous power estimates as also more accurate.

The second conclusion that can be drawn from those simulations is that even though case A and case C are in the same locations there are some differences on their impact on the flow. For example the maximal wake is much larger for case C, but there is a more noticeable drop in relative velocity in case A directly when the tidal currents are at its max. Furthermore in case A there is a more noticeable drop in the free surface. This is expected as there are 73 turbines modelled in case A and 250 in case C

Finally, looking at the mean power extracted by the turbines we see that the 73 turbines of case A produce 0.68 MW/TEC, the 28 turbines of case B produce 0.71 MW/TEC and the 250 turbines of case C produce 0.75 MW/TEC. This means that in this region turbines should produce about 0.7 MW/TEC. However there seems to be a small scale effect, but the power output per turbine is more dependent on the position of the array than the number of turbines or disposition of these. In addition there seems to be a great disparity between the performance during spring and neap tides (as is expected as the power is dependent to the cube of the velocities).

4 PAIMPOL-BREHAT

Only available to PerAWaT participants.

5 MODEL VALIDITY

The validity of the model to represent the initial flow conditions have been studied in WG3 WP3 D1. Simulations outputs were compared to measurements (ADCPs, tidal gauges) to lead to a quantitative assessment of the reliability of the model results (cf. [A2]). The accuracy and the level of confidence of the models will increase with the length and the quality of the measurements.

As, so far, no on site measurements are available to define a reference for tidal farm induced wake or further large scale impact, the proposed approached to integrate tidal farm into TELEMAC system was verified by comparing model outputs to (see WG3 WP3 D2 report [A5]) :

- Experimental data from model test study of the wake induced by a vertical cylinder;
- EDF model test measurements;
- University of Manchester model test measurements;
- University of Edinburgh CFD numerical model results.

Additional details on the validation results can be found in WG3 WP3 D2 [A5].

The models are therefore considered reliable to represent hydrodynamic effects of tidal farm on the initial flow conditions as:

- The modelling of the initial flow conditions was quantified and confirmed in WG3 WP3 D1 [A2];
- The representation of the tidal farm within the TELEMAC system was validated and quantified in WG3 WP3 D2 [A5].

However the validity of the global approach (real site basin scale hydrodynamic modelling + implementation of parametric characterisation of tidal turbines) cannot be specifically quantified as no on site measurements are, at the time being, available.

The representation and implementation of the hydrodynamic effects of tidal farms on real flow conditions is still a research subject. Indeed, physical mechanisms are still to be better understood. A notable example is the importance of turbulence effects. [A6] proposes formulations of average hydrodynamic force and available power estimates that are significantly dependent on turbulence intensity. More generally, more on site (turbine deployments) or laboratory observations are needed to inform the complex nature of fluid-structure interactions in a multi-scale turbulent and transient flow.

Other areas for development:

- Drag and power coefficients are not dependent on incident tidal current direction. These parameters are thought as second order effects, but should be subject to more detailed analysis.
- In this study, only tidal forcing is accounted for, whereas waves or meteorological (wind, atmospheric pressure) may impact the tidal resource and thus impact the characterisation of the fluid – structure interaction.
- The importance of stable numerical schemes has been shown in this study to perform comparative analysis. This issue is integrated in the continuous development and updating of hydrodynamic codes.

6 REFERENCES

[A1] Simon B. (2007). La marée océanique côtière. Institut océanographique éditeur, p. 280.

[A2] Martin V., Pham C.-T., Saviot S. (2012). PerAWaT WG3 WP3 D1 - Tidal basin modelling: The Alderney Race, the Pentland Firth and the Paimpol-Bréhat sites modelled in Telemac software. PerAWaT report.
[A3] Andreewsky M., Joly A., Pham C.-T., Saviot S. (2012). PerAWaT WG3 WP3 D3 - Tidal farm modelling: The Alderney Race, the Pentland Firth and the Paimpol-Bréhat sites modelled in Telemac software. PerAWAT report.
[A4] SHOM (2001). Annuaire des marées pour l'année 2001 – Tome 1 Ports de France.
[A5] Andreewsky M., Bozonnet P., Leonard C. (2012). PerAWAT WG3 WP3 D2 – Code development in TELEMAC2D and TELEMAC3D in order to allow for the implementation of parametric characterisation of arrays. PerAWaT report.
[A6] Neary, V.S., Gunawan, B., Sales D.C. (2013). Turbulent inflow characteristics for hydrokinetic energy conversion in rivers. Renewable and Sustainable Energy Reviews 26 (2013) 437–445.

7 APPENDICE A1: NUMERICAL NOISE

In addition to the hydrodynamics effects analysed in the core of the text, additional perturbations were observed in localised areas of the domain. They concern both free surface elevation and current speed. But the frequency of the perturbations and their very limited extent tend to demonstrate that such perturbations are induced by numerical noise despite the specific use of quasi-bubble discretisation scheme (see [A3]).

Figure 47 shows such perturbation of free surface elevation. It is localised in the bay of Fresnaye. The nature of the oscillations is quantified by the plot of surface elevation time-series (Figure 48). The frequency of the perturbation is rather chaotic and is uncorrelated to the tidal forcing. Another example of numerical noise perturbations is given by Figure 49 and Figure 50. The currents speeds are dramatically modified close to the eastern boundary of the model with high amplitude. Tidal current speed time-series shows that the evolution does not follow in any way the tidal forcing with very sporadic and high amplitudes events.

More investigation should be carried out to assess the influence of numerical parameters on the stability of the results.

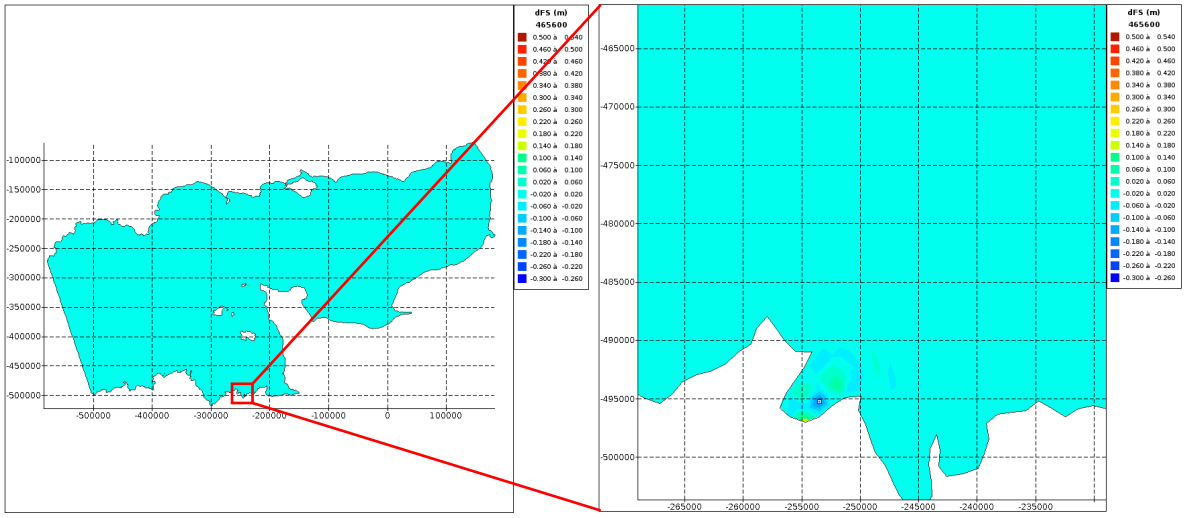

Figure 47: Maps of difference in free surface, dFS (m), global view (left panel) and detailed view on localised variations (right panel).

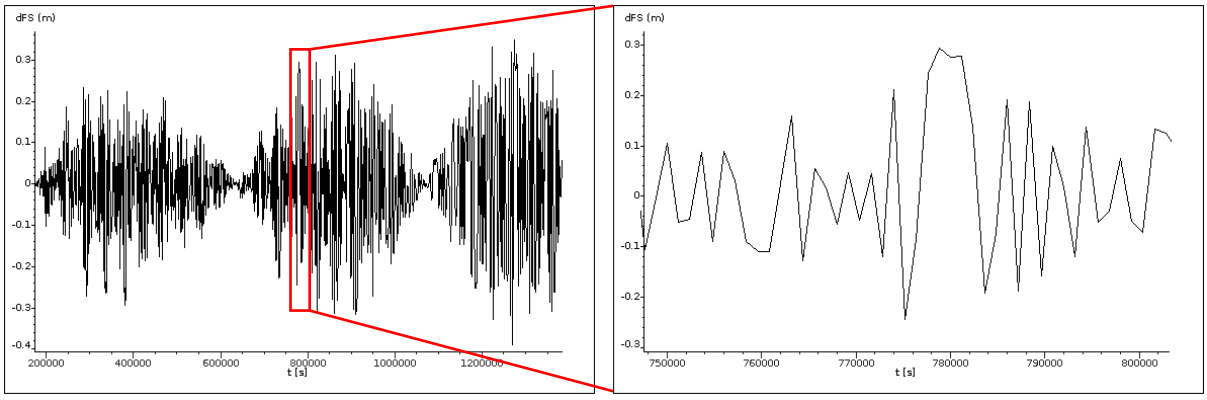

Figure 48: Time variation of difference in free surface, dFS (m), all along the 14-day period (left panel) and during a shorter arbitrary period (right panel).

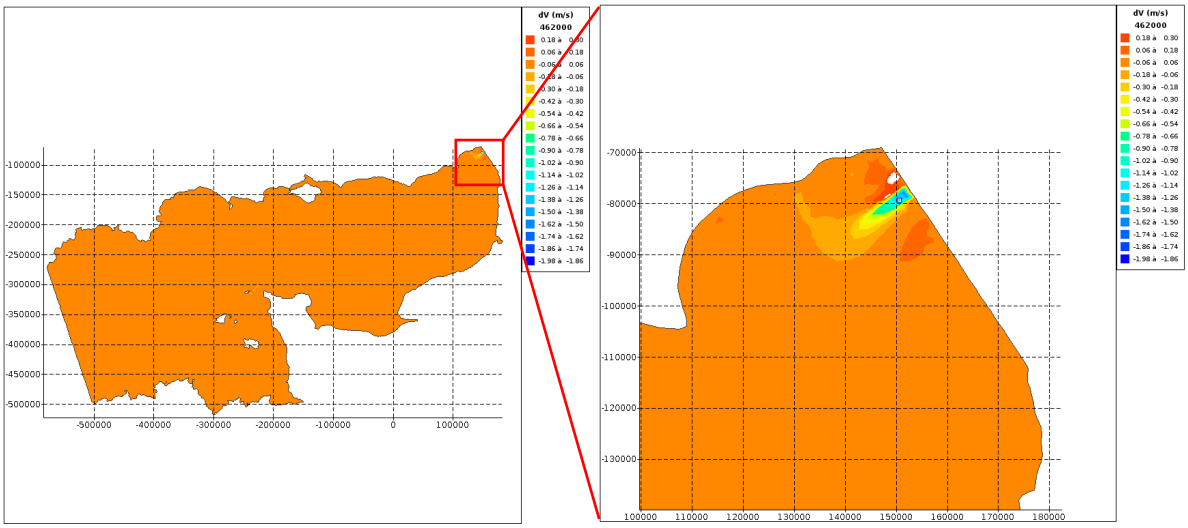

Figure 49: Maps of difference in tidal current velocity, dV (m/s), global view (left panel) and detailed view on localised variations (right panel).

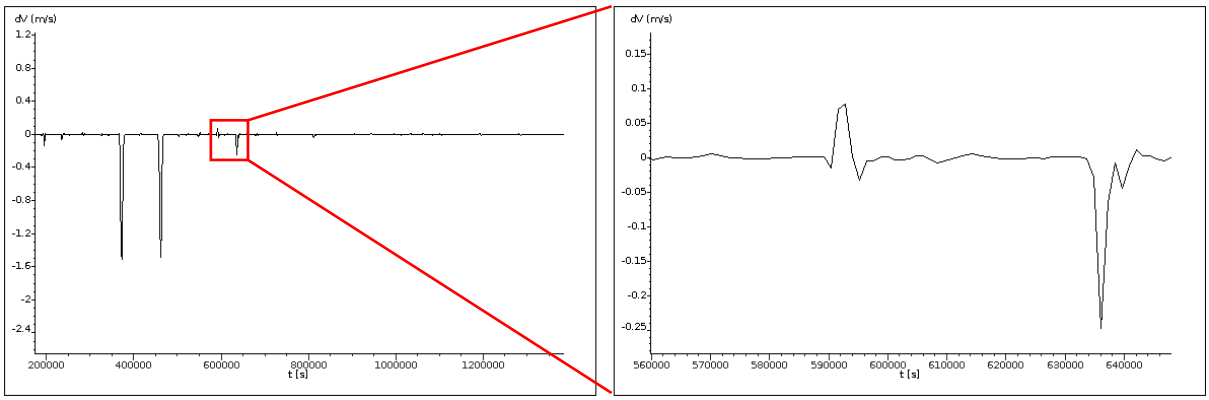

Figure 50: Time variation of difference in tidal current velocity, dV (m/s), all along the 14-day period (left panel) and during a shorter arbitrary period (right panel).